arXiv:astro-ph/0008146v2 14 Mar 2001

# Dust Grain Size Distributions and Extinction in the Milky Way, LMC, and SMC

**DRAFT: 2008.2.1.1450**

Joseph C. Weingartner

*Physics Dept., Jadwin Hall, Princeton University, Princeton, NJ 08544, USA; CITA, 60 St. George Street, University of Toronto, Toronto, ON M5S 3H8, Canada; weingart@cita.utoronto.ca*

and

B.T. Draine

*Princeton University Observatory, Peyton Hall, Princeton, NJ 08544, USA; draine@astro.princeton.edu*

## ABSTRACT

We construct size distributions for carbonaceous and silicate grain populations in different regions of the Milky Way, LMC, and SMC. The size distributions include sufficient very small carbonaceous grains (including polycyclic aromatic hydrocarbon molecules) to account for the observed infrared and microwave emission from the diffuse interstellar medium. Our distributions reproduce the observed extinction of starlight, which varies depending upon the interstellar environment through which the light travels. As shown by Cardelli, Clayton & Mathis in 1989, these variations can be roughly parameterized by the ratio of visual extinction to reddening, $R_V$. We adopt a fairly simple functional form for the size distribution, characterized by several parameters. We tabulate these parameters for various combinations of values for $R_V$ and $b_{\rm C}$, the C abundance in very small grains. We also find size distributions for the line of sight to HD 210121, and for sightlines in the LMC and SMC. For several size distributions, we evaluate the albedo and scattering asymmetry parameter, and present model extinction curves extending beyond the Lyman limit.

*Subject headings:* dust — extinction — ISM: clouds — Magellanic Clouds

## 1. Introduction

Mathis, Rumpl, & Nordsieck (1977, MRN) constructed their classic interstellar dust model on the basis of the observed extinction of starlight for lines of sight passing through diffuse clouds. Strong absorption is observed at 9.7 and 18$\mu$m, corresponding to stretching and bending modes in silicates. The strong extinction feature at 2175 Å can be approximately reproduced by small

graphite particles (Stecher & Donn 1965; Wickramasinghe & Guillaume 1965). The simplest model incorporating both silicate and graphite material consists of two separate grain populations, one of silicate composition and one of graphite composition. MRN found that the extinction curve (i.e. the functional dependence of the extinction on the wavelength $\lambda$) is well reproduced if the grain size distribution (with identical form for each component) is given by

$$dn_{\rm gr} = Cn_{\rm H}a^{-3.5}da, \qquad a_{\rm min} < a < a_{\rm max} \tag{1}$$

with $a_{\rm min} = 50\,\text{Å}$ and $a_{\rm max} = 0.25\mu$m; $n_{\rm gr}(a)$ is the number density of grains with size $\leq a$ and $n_{\rm H}$ is the number density of H nuclei (in both atoms and molecules). MRN adopted spherical grains, for which Mie theory can be used to compute extinction cross sections, and we shall do the same; in this case $a$ is the grain radius. Draine & Lee (1984) extended the wavelength coverage of the MRN model, constructed dielectric functions for "astronomical silicate" and graphite, and found the following normalizations for the size distribution: $C = 10^{-25.13}$ ($10^{-25.11}$) cm$^{2.5}$ for graphite (silicate).

Since the development of the MRN model, more observational evidence has become available; some of these new observations require revisions of the model. First, the extinction curve has been found to vary, depending upon the interstellar environment through which the starlight passes. Cardelli, Clayton, & Mathis (1989, CCM) found that this dependence can be characterized fairly well by a single parameter, which they took to be $R_V \equiv A(V)/E(B-V)$, the ratio of visual extinction to reddening. CCM have fitted the average extinction curve $A(\lambda)/A(V)$ as functions of $\lambda$ and $R_V$. For the diffuse ISM, $R_V \approx 3.1$; higher values are observed for dense clouds. Kim, Martin, & Hendry (1994) used the maximum entropy method to find smooth size distributions, for silicate and graphite grains, for which the extinction for $R_V = 3.1$ and 5.3 is well reproduced. Their $R_V = 5.3$ distribution has significantly fewer "small" grains ($a < 0.1\mu$m) than their $R_V = 3.1$ distribution, as well as a modest increase at larger sizes. This result was expected, since generally there is relatively less extinction at short wavelengths (provided by small grains) for larger values of $R_V$.

Observations of thermal emission from dust have provided another challenge to the MRN model. Emission in the 3 to 60$\mu$m range, presumably generated by grains small enough to reach temperatures of 30 to 600 K or more upon the absorption of a single starlight photon (see e.g. Draine & Anderson 1985), imply a population of very small grains (with $a < 50\,\text{Å}$). The non-detection of the 10$\mu$m silicate feature in emission from diffuse clouds (Mattila et al. 1996; Onaka et al. 1996) appears to rule out silicate grains as a major component of the $a \lesssim 15\,\text{Å}$ population (but see note added in proof). Emission features at 3.3, 6.2, 7.7, 8.6, and 11.3$\mu$m (see Sellgren 1994 for a review) have been identified as C-H and C-C stretching and bending modes in polycyclic aromatic hydrocarbons (Léger & Puget 1984), suggesting that the carbonaceous grain population extends down into the molecular regime. Recent observations of dust-correlated microwave emission has been attributed to the very small grain population (Draine & Lazarian 1998a).

The abundance of very small grains required to generate the observed IR emission from the

diffuse ISM is not yet well-known. In the model of Désert, Boulanger, & Puget (1990), polycyclic aromatic hydrocarbon (PAH) molecules with less than 540 C atoms (equal to the number of C atoms in a spherical graphite grain with $a \approx 10\,\text{Å}$) lock up a C abundance[1] of $\approx 4 \times 10^{-5}$. Li & Draine (2001) compare observations of diffuse galactic emission with detailed model calculations for grains heated by galactic starlight and find that a C abundance $\sim$ 4–6 $\times\, 10^{-5}$ is required in hydrocarbon molecules with $\lesssim 10^3$ C atoms. They conclude that the emission is best reproduced if the very small grain population is the sum of two log-normal size distributions:[2]

$$\frac{1}{n_{\rm H}}\left(\frac{dn_{\rm gr}}{da}\right)_{vsg} \equiv D(a) = \sum_{i=1}^{2}\frac{B_i}{a}\exp\left\{-\frac{1}{2}\left[\frac{\ln(a/a_{0,i})}{\sigma}\right]^2\right\} \quad , \qquad a > 3.5\,\text{Å} \tag{2}$$

$$B_i = \frac{3}{(2\pi)^{3/2}}\frac{\exp(-4.5\sigma^2)}{\rho a_{0,i}^3\sigma}\frac{b_{{\rm C},i}m_{\rm C}}{1+{\rm erf}[3\sigma/\sqrt{2}+\ln(a_{0,i}/3.5\,\text{Å})/\sigma\sqrt{2}]} \quad , \tag{3}$$

where $m_{\rm C}$ is the mass of a C atom, $\rho = 2.24\,{\rm g\,cm^{-3}}$ is the density of graphite, $b_{\rm C,1} = 0.75b_{\rm C}$, $b_{\rm C,2} = 0.25b_{\rm C}$, $b_{\rm C}$ is the total C abundance (per H nucleus) in the log-normal populations, $a_{0,1} = 3.5\,\text{Å}$, $a_{0,2} = 30\,\text{Å}$, and $\sigma = 0.4$.

Draine & Lazarian (1998b) estimated the electric dipole radiation from spinning grains, and found that it could account for the dust-correlated component of the diffuse Galactic microwave emission if $b_{\rm C} \approx 2 \times 10^{-5}$. More recent modelling confirms that the microwave emission can be reproduced with $b_{\rm C} \approx 2$–$4 \times 10^{-5}$ (B. T. Draine & A. Li 2001, in preparation).

Our goal here is to find size distributions which include very small carbonaceous grains[3] (in numbers sufficient to explain the observed infrared and microwave emission attributed to this population) and are consistent with the observed extinction, for different values of $R_V$ in the local Milky Way and for regions in the Large and Small Magellanic Clouds. We consider several values of $b_{\rm C}$, since the C abundance in very small grains is not yet established. We discuss the observational constraints and our method for fitting the extinction in §2, present results in §3, and give a discussion in §4. The size distributions obtained here will be employed in separate studies, including an investigation of photoelectric heating by interstellar dust (Weingartner & Draine 2001).

---

[1] By "abundance", we mean the number of atoms of an element per interstellar H nucleus.

[2] The log-normal distribution with $a_{0,1} = 3.5\,\text{Å}$ is required to reproduce the observed 3–25$\mu$m emission, and the $a_{0,1} = 30\,\text{Å}$ component is needed to contribute emission in the DIRBE 60$\mu$m band.

[3] We take "carbonaceous grains" to refer to graphitic grains and PAH molecules. Although not all carbonaceous grains are graphite, we will continue to refer to the dust model considered here as the "graphite/silicate" model, for simplicity.

## 2. Fitting the Extinction

### 2.1. "Observed" Extinction

For the "observed" extinction $A_{\rm obs}(R_V,\lambda)$, we adopt the parametrization given by Fitzpatrick (1999). Bohlin, Savage, & Drake (1978) found that the ratio of the total neutral hydrogen column density $N_{\rm H}$ (including both atomic and molecular forms) to $E(B-V)$ is fairly constant for the diffuse ISM, with value $5.8\times10^{21}\,{\rm cm}^{-2}$. This provides the normalization for the extinction curve: $A(V)/N_{\rm H}=5.3\times10^{-22}\,{\rm cm}^2$. The normalization is less clear for dense clouds, because of the difficulty in measuring $N_{\rm H}$.[4] CCM found that $A(\lambda)/A(I)$ appears to be independent of $R_V$ for $\lambda>0.9\mu$m (= $I$ band), suggesting that the diffuse cloud value of $A(I)/N_{\rm H}=2.6\times10^{-22}\,{\rm cm}^2$ may also hold for dense clouds (see, e.g., Draine 1989); we adopt this normalization.

### 2.2. Functional Form for the Size Distribution

Lacking a satisfactory theory for the size distribution of interstellar dust, we employ functional forms for the distribution which (1) allow for a smooth cutoff for size $a>a_t$, with control of the steepness of this cutoff; and (2) allow for a change in the slope $d\ln n_{\rm gr}/d\ln a$ for $a<a_t$. We adopt the following form:

$$\frac{1}{n_{\rm H}}\frac{dn_{\rm gr}}{da}=D(a)+\frac{C_{\rm g}}{a}\left(\frac{a}{a_{\rm t,g}}\right)^{\alpha_{\rm g}}F(a;\beta_{\rm g},a_{\rm t,g})\times\left\{\begin{array}{ll}1\quad, & 3.5\,{\rm \AA}<a<a_{\rm t,g}\\ \exp\left\{-[(a-a_{\rm t,g})/a_{\rm c,g}]^3\right\} & a>a_{\rm t,g}\end{array}\right. \tag{4}$$

for carbonaceous dust [with $D(a)$ from eq. (2)] and

$$\frac{1}{n_{\rm H}}\frac{dn_{\rm gr}}{da}=\frac{C_{\rm s}}{a}\left(\frac{a}{a_{\rm t,s}}\right)^{\alpha_{\rm s}}F(a;\beta_{\rm s},a_{\rm t,s})\times\left\{\begin{array}{ll}1\quad, & 3.5\,{\rm \AA}<a<a_{\rm t,s}\\ \exp\left\{-[(a-a_{\rm t,s})/a_{\rm c,s}]^3\right\} & a>a_{\rm t,s}\end{array}\right. \tag{5}$$

for silicate dust. The term

$$F(a;\beta,a_{\rm t})\equiv\left\{\begin{array}{ll}1+\beta a/a_{\rm t}\quad, & \beta\geq0\\ (1-\beta a/a_{\rm t})^{-1} & \beta<0\end{array}\right. \tag{6}$$

provides curvature. The form of the exponential cutoff was suggested by Greenberg (1978). The structure of the size distribution $D(a)$ for the very small carbonaceous grains has only a mild effect on the extinction for the wavelengths of interest; we adopt the same values as Li & Draine (2001) for $a_{0,1}=3.5\,{\rm \AA}$, $a_{0,2}=30\,{\rm \AA}$, and $\sigma=0.4$, and the same relative populations in the two log-normal components ($b_{\rm C,1}=0.75b_{\rm C}$, $b_{\rm C,2}=0.25b_{\rm C}$), but will consider different values of $b_{\rm C}$. Thus equation (4) has a total of six adjustable parameters ($b_{\rm C}$, $C_{\rm g}$, $a_{\rm t,g}$, $a_{\rm c,g}$, $\alpha_{\rm g}$, $\beta_{\rm g}$), with another five parameters ($C_{\rm s}$, $a_{\rm t,s}$, $a_{\rm c,s}$, $\alpha_{\rm s}$, $\beta_{\rm s}$) in equation (5) for the silicate size distribution.

[4] Kim & Martin (1996) compiled a set of sight lines for which both $A(V)/N_{\rm H}$ and $R_V$ are observationally determined. Their data are consistent with $A(V)/N_{\rm H}$ being independent of $R_V$, but the uncertainties are large.

### 2.3. Calculating the Extinction from the Model

The extinction at wavelength $\lambda$ is given by

$$A(\lambda) = (2.5\pi \log e) \int d\ln a \frac{dN_{\rm gr}(a)}{da} a^3 Q_{\rm ext}(a,\lambda) \quad , \tag{7}$$

where $N_{\rm gr}(a)$ is the column density of grains with size $\leq a$ and $Q_{\rm ext}$ is the extinction efficiency factor, which we evaluate (assuming spherical grains) using a Mie theory code derived from BHMIE (Bohren & Huffman 1983).

We adopt silicate dielectric functions based on the "astronomical silicate" functions given by Draine & Lee (1984) and Laor & Draine (1993), but differing in the ultraviolet. The "astronomical silicate" dielectric function $\epsilon = \epsilon_1 + i\epsilon_2$ of Draine & Lee (1984), based on laboratory measurements of crystalline olivine in the ultraviolet (Huffman & Stapp 1973), contains a feature at $6.5\mu{\rm m}^{-1}$. Kim & Martin (1995) have pointed out that this feature, which is of crystalline origin, is not present in the observed interstellar extinction or polarization. We have therefore excised this feature from $\epsilon_2$ and "redistributed" the oscillator strength over frequencies between 8 and $10\mu{\rm m}^{-1}$; we then recomputed $\epsilon_1$ using the Kramers-Kronig relation (Draine & Lee 1984). (The resulting "smoothed astronomical silicate" dielectric functions are available at http://www.astro.princeton.edu/∼draine/.)

For carbonaceous grains, we adopt the description given by Li & Draine (2001), in which the smallest grains are PAH molecules, the largest grains consist of graphite, and grains of intermediate size have optical properties intermediate between those of PAHs and graphite. For PAHs, Li & Draine estimate absorption cross sections per C atom, for both neutral and ionized molecules. Li & Draine estimate PAH absorption near 2175 Å by *assuming* that the 2175 Å absorption profile is in large part due to the PAH population; our adopted PAH absorption cross sections near 2175 Å therefore agree – by construction – with the observed 2175 Å profile. We convert to a size-based description by assuming a C density $\rho = 2.24\,{\rm g\,cm^{-3}}$, and we assume that 50% are neutral and 50% are ionized (the ionization state affects the absorption by these grains at $\lambda \gtrsim 0.6\mu$m). We take graphite dielectric functions from Draine & Lee (1984) and Laor & Draine (1993) and adopt the usual "$1/3 - 2/3$" approximation: $Q_{\rm ext} = [Q_{\rm ext}(\epsilon_\parallel) + 2Q_{\rm ext}(\epsilon_\perp)]/3$, where $\epsilon_\parallel$ and $\epsilon_\perp$ are the components of the graphite dielectric tensor for the electric field parallel and perpendicular to the $c$-axis, respectively. Draine & Malhotra (1993) showed that the $1/3 - 2/3$ approximation is sufficiently accurate for extinction curve modelling.

### 2.4. Abundance/Depletion Constraints

Given estimates of the abundances and interstellar depletions of the elements incorporated in dust and the mass densities of the grain materials, we can estimate the total volume per H atom, $V_{\rm tot}$, in the carbonaceous and silicate grain populations. For a long time, solar abundances were used for this purpose (see Grevesse & Sauval 1998 for a recent compendium of solar abundances).

Recent evidence, e.g. from measurements of abundances in the atmospheres of B stars, suggest that the abundances in the present-day ISM may be substantially lower than the solar values (see Snow & Witt 1996; Mathis 1996, 2000; and Snow 2000 for reviews). However, Fitzpatrick & Spitzer (1996) concluded that S has solar abundance in the ISM, and Howk, Savage, & Fabian (1999) found solar abundances of Zn, P, and S along the line of sight to $\mu$ Columbae. Thus, interstellar abundances are not yet well-known.

We adopt the solar C abundance of $3.3 \times 10^{-4}$ (Grevesse & Sauval 1998) and assume that $\approx$ 30% is in the gas phase.[5] With the ideal graphite density of $2.24\,\mathrm{g\,cm^{-3}}$, we find $V_{\rm tot,g} \approx 2.07 \times 10^{-27}\,\mathrm{cm^3\,H^{-1}}$ for carbonaceous dust. To estimate the total volume in amorphous silicates, we assume a stoichiometry approximating $MgFeSiO_4$, with mass number per structural unit of 172. Since Si, Mg, and Fe have similar abundances in the Sun and are all highly depleted in the ISM (Savage & Sembach 1996), we simply assume that the Si abundance in silicate dust is equal to its solar value of $3.63 \times 10^{-5}$. We adopt a density of $3.5\,\mathrm{g\,cm^{-3}}$, intermediate between the values for crystalline forsterite ($Mg_2SiO_4$, $3.21\,\mathrm{g\,cm^{-3}}$) and fayalite ($Fe_2SiO_4$, $4.39\,\mathrm{g\,cm^{-3}}$). Thus, we estimate $V_{\rm tot,s} \approx 2.98 \times 10^{-27}\,\mathrm{cm^3\,H^{-1}}$ for silicate dust.

### 2.5. Method of Solution

For a given pair of values ($R_V$, $b_{\rm C}$), we seek the best fit to the extinction by varying the powers $\alpha_{\rm g}$ and $\alpha_{\rm s}$; the "curvature" parameters $\beta_{\rm g}$ and $\beta_{\rm s}$; the transition sizes $a_{\rm t,g}$ and $a_{\rm t,s}$; the upper cutoff parameters $a_{\rm c,g}$ and $a_{\rm c,s}$; and the total volume per H in both the carbonaceous and silicate distributions, $V_{\rm tot,g}$ and $V_{\rm tot,s}$, respectively.

We use the Levenberg-Marquardt method, as implemented in Press et al. (1992), to fit the continuous extinction between $0.35\mu\mathrm{m}^{-1}$ and $8\mu\mathrm{m}^{-1}$.[6] We evaluate the extinction at 100 wavelengths $\lambda_i$, equally spaced in $\ln\lambda$, and minimize one of two error functions. In the first case (hereafter "case A") we minimize $\chi^2 = \chi_1^2 + \chi_V^2$.

The first term in $\chi^2$ gives the error in the extinction fit:

$$\chi_1^2 = \sum_i \frac{\left(\ln A_{\rm obs} - \ln A_{\rm mod}\right)^2}{\sigma_i^2} \quad , \tag{8}$$

where $A_{\rm obs}(\lambda_i)$ is the average "observed" extinction (§2.1), $A_{\rm mod}(\lambda_i)$ is the extinction computed for the model [equation (7)], and the $\sigma_i$ are weights. When evaluating $A_{\rm mod}$, we verify that the integral

[5] Cardelli et al. (1996) and Sofia et al. (1997) found a gas-phase C abundance of $1.4 \times 10^{-4}$, larger than the $\approx 1 \times 10^{-4}$ that we assume.

[6] The lower limit of $0.35\mu\mathrm{m}^{-1}$ was chosen so as to avoid infrared absorption features, most notably the $3.4\mu$m C-H stretch feature. Extinction data for $\lambda^{-1} > 8\mu\mathrm{m}^{-1}$ are very limited.

in equation (7) is evaluated accurately. We take the weights $\sigma_i^{-1} = 1$ for $1.1\mu\mathrm{m}^{-1} < \lambda^{-1} < 8\mu\mathrm{m}^{-1}$ and $\sigma_i^{-1} = 1/3$ for $\lambda^{-1} < 1.1\mu\mathrm{m}^{-1}$, since the actual IR extinction is uncertain.

The term $\chi_V^2$ is a penalty which keeps the total volumes in the carbonaceous and silicate grain populations from grossly exceeding the abundance/depletion-limited values found in §2.4. We take

$$\chi_V^2 = 0.4[\max(\tilde{V}_\mathrm{g}, 1) - 1]^{1.5} + 0.4[\max(\tilde{V}_\mathrm{s}, 1) - 1]^{1.5} \quad , \tag{9}$$

where $\tilde{V}_\mathrm{g} = V_\mathrm{tot,g}/2.07 \times 10^{-27}\,\mathrm{cm}^3\,\mathrm{H}^{-1}$ and $\tilde{V}_\mathrm{s} = V_\mathrm{tot,s}/2.98 \times 10^{-27}\,\mathrm{cm}^3\,\mathrm{H}^{-1}$.

Given our assumption that $A(I)/N_\mathrm{H}$ is independent of $R_V$, the extinction for higher $R_V$ can be fit using less total grain volume. It seems highly unlikely that material is transferred from grains to the gas phase as gas and dust cycles into regions of higher density. Thus, we also consider a second case ("case B") for which the grain volumes are held fixed at approximately the values found for $R_V = 3.1$: $V_\mathrm{tot,s} = 3.9 \times 10^{-27}\,\mathrm{cm}^3\,\mathrm{H}^{-1}$ and $V_\mathrm{tot,g} = 2.3 \times 10^{-27}\,\mathrm{cm}^3\,\mathrm{H}^{-1}$. In this case, we seek to minimize $\chi_1^2$.

## 3. Results

### 3.1. Dust in the Milky Way

#### *3.1.1. Size Distributions and Extinction Fits*

We have generally found, in fitting the extinction, that $\chi^2$ varies only slightly with the silicate cutoff parameter $a_\mathrm{c,s}$ until $a_\mathrm{c,s}$ exceeds a critical value of $\approx 0.1\mu$m (for Milky Way dust; see Figure 1). As $a_\mathrm{c,s}$ increases, the silicate grains contribute less short-wavelength extinction, and a large abundance of small carbonaceous grains is required to pick up the slack. When $a_\mathrm{c,s} \gtrsim 0.1\mu$m, the 2175 Å hump is overproduced. Although $\chi^2$ is nearly constant for $a_\mathrm{c,s} \lesssim 0.1\mu$m, it does increase slightly with $a_\mathrm{c,s}$. Consequently, our fitting algorithm returns very small values for $a_\mathrm{c,s}$, for which the silicate size distribution drops off very sharply at the large-size end. Since such sharp cutoffs are unlikely to occur in nature, we have opted to fix $a_\mathrm{c,s} = 0.1\mu$m.

In Table 1 we list the values of the distribution parameters for which the extinction with $R_V = 3.1$, 4.0, and 5.5 is best fit, for various values of $b_\mathrm{C}$.[7] These distributions are displayed in Figures 2 through 6.

In Figure 7 we display $A_\mathrm{obs}$ and $A_\mathrm{mod}$ for case A, the three values of $R_V$, and the highest values of $b_\mathrm{C}$ included in Table 1, in a log-log plot, to give a sense for the fit quality over the entire range of $\lambda^{-1}$. In Figures 8 through 12, we display extinction curves for $b_\mathrm{C} = 0$ and for the highest value of $b_\mathrm{C}$ included in Table 1; we show the contribution from each of the grain distribution components.

[7]These parameters [and a FORTRAN subroutine that returns $dn_\mathrm{gr}/da(a)$] are also available in electronic form on the World Wide Web at www.cita.utoronto.ca/∼weingart.

In Table 1 we also display $\chi^2$, $\chi^2_1$, and $\chi^2_2 = \sum_i (\ln A_{\rm obs} - \ln A_{\rm mod})^2$. For a given value of $R_V$, the error functions do not vary substantially with $b_{\rm C}$ until a critical value of $b_{\rm C}$ is reached, at which point the error functions increase dramatically (see Figure 13). Clearly, extinction evidence alone does not constrain $b_{\rm C}$ well except that $b_{\rm C} \lesssim 6 \times 10^{-5}$ for the $R_V = 3.1$ extinction law, $b_{\rm C} \lesssim 4 \times 10^{-5}$ for $R_V = 4$, and $b_{\rm C} \lesssim 3 \times 10^{-5}$ for $R_V = 5.5$. In each case, the upper limit on $b_{\rm C}$ is reached when the very small carbonaceous particles account for 100% of the 2175Å extinction feature.

In assessing the quality of the extinction fits, one must bear in mind that (1) the dielectric functions used are certainly not correct in detail, even for bulk material, (2) the surface monolayers of grains are likely to differ from bulk materials, (3) the true size distributions undoubtedly differ from the adopted functional form, and (4) the interstellar grains are appreciably non-spherical. Therefore, a precise fit is not to be expected. One should also remember that the adopted PAH absorption cross section in the vacuum ultraviolet was constructed to fit the interstellar 2175 Å profile, and the silicate dielectric function in the vacuum ultraviolet was modified to suppress structure not present in the observed interstellar extinction.

### *3.1.2. Further Results*

Although neutral H gas is opaque for wavelengths shortward of the Lyman limit, extinction by dust at such wavelengths could have important observational consequences within ionized regions, including objects at high redshift. Thus, in Figure 14 we plot the model extinction resulting from several of our distributions over an extended wavelength range.

In Figure 15, we plot the albedo and asymmetry parameter $g \equiv \langle \cos\theta \rangle$ (i.e. the average value of $\cos\theta$, where $\theta$ is the angle through which radiation is scattered by dust) resulting from several of our model size distributions.

Since Li & Draine (2001) find that the IR emission from dust in the diffuse ISM is best fit when $b_{\rm C} \approx 6 \times 10^{-5}$, we adopt this value for the $R_V = 3.1$ curves in Figures 14 and 15. For such a large $b_{\rm C}$, the 2175 Å hump is almost entirely due to the very small carbonaceous grain population. If this is the case for the diffuse ISM, then it seems plausible that it also holds in denser regions; i.e., the decrease in the strength of the 2175 Å feature with $R_V$ might result entirely from the depletion of very small carbonaceous grains. Thus, we have also adopted the large-$b_{\rm C}$ distributions for $R_V = 4.0$ and 5.5 in Figures 14 and 15.

### *3.1.3. Dust Along the Line of Sight to HD 210121*

Although the variation of the extinction curve with interstellar environment is fairly well characterized by the CCM parameterization, there are lines of sight for which the extinction deviates substantially from CCM. As a further test of the bare carbonaceous/silicate dust model, it is

important to seek size distributions which can reproduce the extinction along such sightlines. The extinction observed toward HD 210121 (a sightline passing through a high-latitude diffuse molecular cloud) has (1) an extremely small value of $R_V = 2.1$, (2) a 2175 Å feature weaker than predicted by the CCM parameterization, and (3) a stronger-than-expected far-UV rise (see Figure 1 in Larson et al. 2000). This sightline therefore provides an opportunity to test the carbonaceous/silicate model and the functional forms used for our size distributions.

Larson et al. (2000) used the maximum entropy method to construct size distributions for the grains toward HD 210121. We seek to reproduce the extinction toward HD 210121 (Larson et al. 2000; Larson, Whittet, & Hough 1996; Welty & Fowler 1992) with size distributions of our simple functional form. We adopt the normalization given by Larson et al. (2000): $A_V/N_{\rm H} = 3.6 \times 10^{-22}\,{\rm cm}^2$. In fitting the extinction, we adopt 100 points equally spaced in $\lambda^{-1}$ rather than in $\ln\lambda$. We have found that this yields a better fit to the 2175 Å hump and far-UV rise without compromising the fit quality in the infrared. Distribution parameter values are given in Table 2 and the distributions and extinction fits are plotted in Figures 16 and 17, respectively.

We are able to obtain acceptable fits to the extinction toward HD 210121 with values of $b_c$ ranging up to $4 \times 10^{-5}$, and reasonable size distributions for the carbonaceous and silicate grain populations. Our grain model successfully accomodates this line of sight with its extremely small value of $R_V$ and deviation from the CCM parameterization.

### 3.2. Dust in the Magellanic Clouds

The metallicities in the Magellanic Clouds are substantially lower than in the Milky Way, and measured extinction curves toward stars in the LMC and SMC differ from typical extinction curves in the Milky Way. The LMC and SMC therefore offer opportunities to test the applicability of our grain model to low-metallicity extragalactic environments.[8]

Clayton et al. (2000) used the maximum entropy method to find graphite/silicate size distributions that accurately reproduce the extinction along various Magellanic Cloud sightlines. Here, we seek distributions of our simple functional form that reproduce the average extinction in the LMC (Misselt, Clayton, & Gordon 1999), the extinction in the LMC 2 area (Misselt et al. 1999), and the extinction in the SMC bar, along the line of sight to the star AzV398 (Gordon & Clayton 1998). For $\lambda^{-1} \lesssim 3\mu{\rm m}^{-1}$, the extinction is determined at only a small number of wavelengths. Thus, for the Magellanic Clouds, we evaluate the extinction at 100 wavelengths spaced equally in $\lambda^{-1}$, rather than in $\ln\lambda$.

The extinction normalization and elemental abundances are even more uncertain for the Magellanic clouds than for the Milky Way. For the LMC, Koorneef (1982) found $N({\rm H\,I})/E(B-V) =$

[8]See Pei (1992) for an early extension of the MRN model to the Magellanic Clouds.

$2.0 \times 10^{22}\,\mathrm{cm}^{-2}$ and Fitzpatrick (1985) found $N(\mathrm{H\,I})/E(B-V) = 2.4 \times 10^{22}\,\mathrm{cm}^{-2}$. Averaging these results and taking $R_V = 2.6$ (the average for the 10 measured $R_V$ values in Misselt et al.'s sample), we adopt $A(V)/N_\mathrm{H} = 1.2 \times 10^{-22}\,\mathrm{cm}^2$. For the SMC, Martin, Maurice, & Lequeux (1989) found $N_\mathrm{H}/E(B-V) = 4.6 \times 10^{22}\,\mathrm{cm}^{-2}$; with $R_V = 2.87$ (Gordon & Clayton 1998) this yields $A(V)/N_\mathrm{H} = 6.2 \times 10^{-23}\,\mathrm{cm}^2$. We take the abundance/depletion-limited values of $V_\mathrm{tot,g}$ and $V_\mathrm{tot,s}$ to be reduced from their values in the Milky Way by a factor 1.6 for the LMC and 4.0 for the SMC (Gordon & Clayton 1998).

Distribution parameters for which the extinction is best fit are given in Table 3. We also tabulate the total grain volumes, normalized to the limiting values estimated in the previous paragraph; note that all of the LMC distributions use less than the estimated available amount of C and Si. Size distributions, extinction fits, and related quantities are plotted in Figures 18 through 23.

Note the absence of the 2175 Å feature in the SMC bar extinction curve (Figure 21), which implies the absence of very small carbonaceous grains. Recently, Reach et al. (2000) have detected PAH emission features in a quiescent molecular cloud in the SMC. Reach et al. point out that SMC extinction curve measurements are biased towards hot, luminous stars, so that very small grains may have been destroyed along these sightlines.

## 4. Discussion

### 4.1. Abundances and Grain Models

Note from Table 1 that, in the Milky Way, the silicate volumes generally exceed the abundance/depletion-limited value, by $\approx 10\%$ when $R_V = 5.5$ to $\approx 30\%$ when $R_V = 3.1$, and the carbonaceous grain volume exceeds its abundance/depletion-limited value by $\approx 10\%$ when $R_V = 3.1$. We would expect non-spherical grains to produce more extinction per unit grain volume than spheres, so that our violation of abundance constraints might be an artifact due to the use of only spherical grains in our modelling. However, we have used the discrete dipole approximation (Draine & Flatau 1994; Draine 2000) to calculate extinction efficiencies for silicate grains of various shapes with $a \geq 0.01\mu$m and have found that the integrated extinction per grain volume, $\int (C_\mathrm{ext}/V) d\lambda$ integrated over $\lambda^{-1} \in [0.35, 8.0]\mu\mathrm{m}^{-1}$, varies only slightly with shape.

Kim et al. (1994) sought to maximize the efficient use of grain volume by allowing more complicated size distributions. Although such an approach could lower the total amount of grain volume that we need to reproduce the observed extinction, we find such fine-tuning unappealing. It seems to us unlikely that nature has produced size distributions fine-tuned to maximize the extinction per volume over just the wavelengths where we are able to measure the extinction. We think it more likely that either the true elemental abundances in the ISM really are somewhat higher than in the Sun, or that the bare graphite/silicate model is inadequate in some more fundamental way.

Other well-developed models include composite, fluffy grains (Mathis 1996, 1998) and grains consisting of silicate cores covered by organic refractory mantles (Li & Greenberg 1997). The recent discovery that the 3.4$\mu$m aliphatic C-H stretch absorption feature toward Sgr A IRS7 is unpolarized (whereas the 9.7$\mu$m silicate absorption feature toward Sgr A IRS3 is polarized) may rule out the core-mantle model (Adamson et al. 1999), although model calculations of the relative polarization in these features have not yet been carried out for the core-mantle model, and the silicate feature polarization has yet to be measured for IRS 3 itself.

Mathis (1996) found that a mixture of composite grains (consisting of small silicate and amorphous carbon grains and $\approx 45\%$ vacuum), small graphite grains, and some small silicate grains could reproduce the observed extinction while incorporating C, Si, Fe, and Mg with substantially sub-solar abundances. However, there are some difficulties with this model. First, Mathis adopts dielectric functions for the composite grains using effective medium theory, calculates extinction cross sections for spheres, and then multiplies the cross sections by a factor 1.09, to account for enhancements in extinction due to non-spherical shapes. The final step must be viewed with suspicion, since it fails for compact silicate grains.

Also, Mathis used the optical properties of "Be" amorphous carbon from Rouleau & Martin (1991). Schnaiter et al. (1998) have pointed out that the derived optical properties, while possibly correct, are unproven, since the adopted description of the sample geometry as a continuous distribution of ellipsoids is so simplistic that substantial errors can result. Furthermore, "Be" amorphous carbon is much more absorbing at long wavelengths than various forms of hydrogenated amorphous carbon, and this absorption provides most of the extinction for $\lambda^{-1} \lesssim 3\mu\mathrm{m}^{-1}$ in the Mathis (1996) composite model.[9] Furton, Laiho, & Witt (1999) have performed laboratory studies of hydrogenated amorphous carbon, and find that such grains can reproduce the observed 3.4$\mu$m absorption feature if the degree of hydrogenation is rather large ($\approx 0.5\,\mathrm{H/C}$). There is very little visible/IR continuum absorption in this case. Thus, the composite model does not simultaneously provide enough long-wavelength extinction and 3.4$\mu$m absorption. Of course, the bare graphite/silicate model does not account for the 3.4$\mu$m absorption either.[10]

Although the bare graphite/silicate model apparently requires higher abundances of C, Si, Fe, and Mg than are generally thought to be available in the ISM, it would be premature to abandon it. The true interstellar abundances are not yet known, and the alternatives have difficulties too. Further progress in dust modelling will require the determination of dielectric functions for amorphous carbons with a range of degrees of hydrogenation, over the full range $\lambda^{-1} \in [0.35, 8.0]\mu\mathrm{m}^{-1}$, as well as detailed modelling of how the extinction per unit volume varies depending on grain geometry.

---

[9]Dwek (1997) has argued that the fluffy grain model employing "Be" amorphous carbon produces too much IR emission compared with the COBE data (Dwek et al. 1997).

[10]To accomodate the 3.4$\mu$m feature, the graphite/silicate model must be extended to include aliphatic hydrocarbons, possibly within hydrogenated carbon coatings on the large graphitic grains.

### 4.2. Observed Size Distribution of Interstellar Grains Streaming Through the Solar System

Recently, Frisch et al. (1999) have presented a grain mass distribution for the local interstellar medium (LISM), derived from the measured rate of impact of interstellar grains with detectors on the *Ulysses* and *Galileo* spacecraft; we reproduce their data points in Figure 24. We also show mass distributions as derived here from fitting extinction, for $(R_V, 10^5 b_{\rm C}) = (3.1,\ 3.0)$, $(4.0,\ 2.0)$, and $(5.5,\ 1.0)$. We adopt $n_{\rm H} = 0.3\,{\rm cm}^{-3}$, as recommended by Frisch et al. Note that none of our distributions resemble the Frisch et al. result. The steep drop in the Frisch et al. distribution at small masses probably reflects the exclusion of small grains from the solar system – smaller grains are more tightly coupled to the magnetic field and are less likely to penetrate the heliosphere to within $\sim 5\,{\rm AU}$ of the Sun (Linde & Gombosi 2000). However, the large amount of mass in large grains in the Frisch et al. distribution is hard to fathom. The error bars on the Frisch et al. data (not shown in Figure 24) are large; further observations of interstellar dust entering the solar system would be of great value.

If the Frisch et al. result is confirmed, then there are two possibilities. If the region through which the solar system is now passing contains a truly representative dust-gas mixture, then a dramatically different grain model would be required. It is difficult to envision a grain model which could simultaneously account for the interstellar extinction law, be consistent with interstellar elemental abundances, and reproduce the Frisch et al. size distribution. Alternatively, it could be the case that size-sorting and gas-grain separation occur on small scales in the ISM, and that the region through which the solar system is now moving happens to have an unusual concentration of large grains.

### 4.3. Conclusions

The simplest interstellar dust model consists of a population of carbonaceous grains and a separate population of silicate grains. In the original development of this model by MRN, the grain size distribution was chosen so as to reproduce the observed extinction for lines of sight with $R_V \approx 3.1$. The observation of relatively short-wavelength infrared emission from dust implies that there are substantial numbers of very small (mainly carbonaceous) grains, smaller than the lower cutoff size of the MRN distribution. Furthermore, the extinction curve has been found to vary substantially depending on the interstellar environment through which the starlight passes; thus, there is no single grain size distribution which applies in all environments. By finding carbonaceous/silicate grain size distributions which contain sufficient very small grains to account for the observed infrared emission (Li & Draine 2001), and which reproduce the observed extinction for a wide range of environments, we have demonstrated that the simplest dust model remains viable.

Although difficulties remain, they are no more severe than the difficulties with other, more complicated, models. These difficulties include the requirement of somewhat super-solar abun-

dances of the dust constituent elements, the lack of a 3.4$\mu$m absorption feature in a model in which all of the C is in graphite or PAHs, and the gross disparity between the derived grain size distributions and that inferred by Frisch et al. (1999) for dust in the local ISM. Additionally, there is evidence from depletion patterns that metallic Fe or Fe oxides are an important dust component (Sofia et al. 1994; Howk et al. 1999). The observed 90 GHz emission from interstellar dust appears to rule out a substantial metallic Fe component (Draine & Lazarian 1999), but oxides such as FeO or magnetite $Fe_3O_4$ are not excluded. Dielectric functions for candidate Fe oxides are needed to investigate such grain models.

Finally, the variation in the grain size distribution with environment seems to indicate that small grains coagulate onto large grains in relatively dense environments, as expected (Draine 1985; Draine 1990). Presumably, mass is returned from large to small grains via shattering during grain-grain collisions in shock waves. (Mass is also returned to the gas via sputtering processes.) Weingartner & Draine (1999) found that the observed elemental depletions in the interstellar medium could be due to accretion onto grains if the timescales for matter to cycle between interstellar phases are $\sim 10^7$ yr. It remains a mystery how two separate grain populations – carbonaceous grains and silicate grains – could remain distinct after evolving through many cycles of coagulation, shattering, accretion, and erosion; perhaps they do not.

While real grains are undoubtedly more complex, the graphite/silicate model for dust in diffuse clouds is clearly-defined, and consistent with observations of interstellar extinction in the Milky Way, LMC, and SMC (as demonstrated in the present work) and infrared emission (Li & Draine 2001). While the model does not explicitly account for the 3.4$\mu$m feature or the relatively weak diffuse interstellar bands (Herbig 1995), these could conceivably be accomodated by modest modifications of or extensions to the basic graphite/silicate model. The "extended red emission" from interstellar dust (Witt & Boroson 1990) could also perhaps be due to a minor modification of the basic graphite/silicate model (e.g., a hydrogenated amorphous carbon coating; Witt & Furton 1995).

Until a more compelling grain model is available, we recommend the use of the simplest one, specified by the size distributions found here and optical properties given by Draine & Lee (1984), Laor & Draine (1993), and Li & Draine (2001). In particular, we favor the distributions with relatively large $b_C$ (Li & Draine 2001), for which the very small carbonaceous grain population entirely accounts for the 2175 Å hump in the extinction curve.

This research was supported in part by NSF grant AST-9619429 and by NSF Graduate and International Research Fellowships to JCW. We are grateful to Eli Dwek, Aigen Li, and John Mathis for helpful discussions and to R. H. Lupton for the availability of the SM plotting package.

## REFERENCES

Adamson, A. J., Whittet, D. C. B., Chrysostomou, A., Hough, J. H., Aitken, D. K., Wright, G. S., & Roche, P. F. 1999, ApJ, 512, 224

Bohlin, R. C., Savage, B. D., & Drake, J. F. 1978, ApJ, 224, 132

Bohren, C. F. & Huffman, D. R. 1983, Absorption and Scattering of Light by Small Particles (New York: Wiley)

Cardelli, J. A., Clayton, G. C., & Mathis, J. S. 1989 (CCM), ApJ, 345, 245

Cardelli, J.A., Meyter, D.M., Jura, M., Savage, B.D. 1996, ApJ, 467, 334

Clayton, G. C., Wolff, M. J., Gordon, K. D., & Misselt, K. A. 2000, in Thermal Emission Spectroscopy and Analysis of Dust, Disks, and Regoliths, ed. M. L. Sitko, A. L. Sprague, & D. K. Lynch, ASP Conf. Series, 196, 41

Désert, Boulanger, & Puget 1990, A&A, 237, 215

Draine, B. T. 1985, in Protostars and Planets II, ed. D. C. Black & M. S. Matthews (Tucson: Univ. of Arizona Press), p. 621

Draine, B. T. 1989, in Infrared Spectroscopy in Astronomy, ed. B. H. Kaldeich (Paris: ESA), 93

Draine, B. T. 1990, in The Evolution of the Interstellar Medium, ed. L. Blitz, ASP Conf. Series, 12, 193

Draine, B. T. 2000, in Light Scattering by Nonspherical Particles: Theory, Measurements, and Applications, ed. M. I. Mishchenko, J. W. Hovenier, & L. D. Travis (N.Y.: Academic Press), p. 131

Draine, B. T. & Anderson, N. 1985, ApJ, 292, 494

Draine, B. T., & Flatau, P. J. 1994, J. Opt. Soc. Am., A, 11, 1491

Draine, B. T. & Lazarian, A. 1998a, ApJ, 494, L19

Draine, B. T. & Lazarian, A. 1998b, ApJ, 508, 157

Draine, B. T., & Lazarian, A. 1999, ApJ, 512, 740

Draine, B. T. & Lee, H. M. 1984, ApJ, 285, 89

Draine, B. T., & Li, A. 2000, in preparation

Draine, B. T., & Malhotra, S. 1993, ApJ, 414, 632

Dwek, E. 1997, ApJ, 484, 779

Dwek, E. et al. 1997, ApJ, 475, 565

Fitzpatrick, E. L. 1985, ApJ, 299, 219

Fitzpatrick, E. L. 1999, PASP, 111, 63

Fitzpatrick, E. L., & Spitzer, L. Jr. 1996, ApJ, 475, 623

Frisch, P. C., et al. 1999, ApJ, 525, 492

Furton, D. G., Laiho, J. W., & Witt, A. N. 1999, ApJ, 526, 752

Gordon, K. D. & Clayton, G. C. 1998, ApJ, 500, 816

Greenberg, J. M. 1978, in Cosmic Dust, ed. J. A. M. McDonnell (Chichester: Wiley), 187

Grevesse, N. & Sauval, A. J. 1998, Space Sci. Rev., 85, 161

Herbig, G. H. 1995, ARAA, 33, 19

Howk, J. C., Savage, B. D., & Fabian, D. 1999, ApJ, 525, 253

Kim, S.-H. & Martin, P. G. 1995, ApJ, 442, 172

Kim, S.-H. & Martin, P. G. 1996, ApJ, 462, 296

Kim, S.-H., Martin, P. G., & Hendry, P. D. 1994, ApJ, 422, 164

Koorneef, J. 1982, A&A, 107, 247

Laor, A. & Draine, B. T. 1993, ApJ, 402, 441

Larson, K. A., Whittet, D. C. B., & Hough, J. H. 1996, ApJ, 472, 755

Larson, K. A., Wolff, M. J., Roberge, W. G., Whittet, D. C. B., & He, L. 2000, ApJ, 532, 1021

Léger, A. & Puget, J. L. 1984, A&A, 137, L5

Li, A. & Draine, B. T. 2000 [astro-ph/0012147]

Li, A. & Draine, B. T. 2001, ApJ, submitted [astro-ph/0011319]

Li, A. & Greenberg, J. M. 1997, A&A, 323, 566

Linde, T. J., & Gombosi, T. I. 2000, JGR, A5, 10411

Martin, N., Maurice, E., & Lequeux, J. 1989, A&A, 215, 219

Mathis, J. S. 1996, ApJ, 472, 643

Mathis, J. S. 1998, ApJ, 497, 824

Mathis, J. S. 2000, JGR, 105, A5, 10269

Mathis, J. S., Rumpl, W., & Nordsieck, K. H. 1977, ApJ, 217, 425

Mattila, K., Lemke, D., Haikala, L. K., Laureijs, R. J., Léger, A., Lehtinen, K., Leinert, Ch., & Mezger, P. G. 1996, A&A, 315, L353

Misselt, K. A., Clayton, G. C., & Gordon, K. D. 1999, ApJ, 515, 128

Onaka, T., Yamamura, I., Tanabé, T., Roellig, T. L., & Yuen, L. 1996, PASJ, 48, L59

Pei, Y. C. 1992, ApJ, 395, 130

Press, W. H., Teukolsky, S. A., Vetterling, W. T., & Flannery, B. P. 1992, Numerical Recipes in FORTRAN: The Art of Scientific Computing, Second Edition (Cambridge: Cambridge University Press)

Reach, W. T., Boulanger, F., Contursi, A., & Lequeux, J. 2000, A&A, submitted

Rouleau, F. & Martin, P. G. 1991, ApJ, 377, 526

Savage, B.D., & Sembach, K.R. 1996, ARAA, 34, 279

Schnaiter, M., Mutschke, H., Dorschner, J., Henning, Th., & Salama, F. 1998, ApJ, 498, 486

Sellgren, K., 1994, in The Infrared Cirrus and Diffuse Interstellar Clouds, ed. R. Cutri & W. B. Latter, A.S.P. Conference Series, 58, 243

Snow, T. P. & Witt, A. N. 1996, ApJ, 468, L65

Snow, T. P. 2000, JGR, 105, A5, 10239

Sofia, U.J., Cardelli, J.A., Guerin, K.P., Meyer, D.M. 1997, ApJ, 482, L105

Stecher, T. P. & Donn, B. 1965, ApJ, 142, 1683

Weingartner, J. C. & Draine, B. T. 1999, ApJ, 517, 292

Weingartner, J.C., & Draine, B.T. 2001, ApJS, 135,000 [astro-ph/9907251]

Welty, D. E. & Fowler, J. R. 1992, ApJ, 393, 193

Wickramasinghe, N. C. & Guillaume, C. 1965, Nature, 207, 366

Witt, A. N., & Boroson, T. A. 1990, ApJ, 355, 182

Witt, A. N., & Furton, D. G. 1995, in The Diffuse Interstellar Bands, eds. A. G. G. M. Tielens & T. P. Snow, (Dordrecht: Kluwer), p. 149

Note added in proof—Li & Draine (2000) have recently found that the nondetection of the $10\mu$m silicate feature in emission from diffuse clouds does not strongly constrain the ultrasmall silicate grain population, since the $10\mu$m feature may be hidden by the dominant PAH features. Li & Draine estimate that as much as $\sim 20\%$ of the interstellar Si could be in grains with $a \lesssim 15\,\text{Å}$.

This preprint was prepared with the AAS LaTeX macros v5.0.

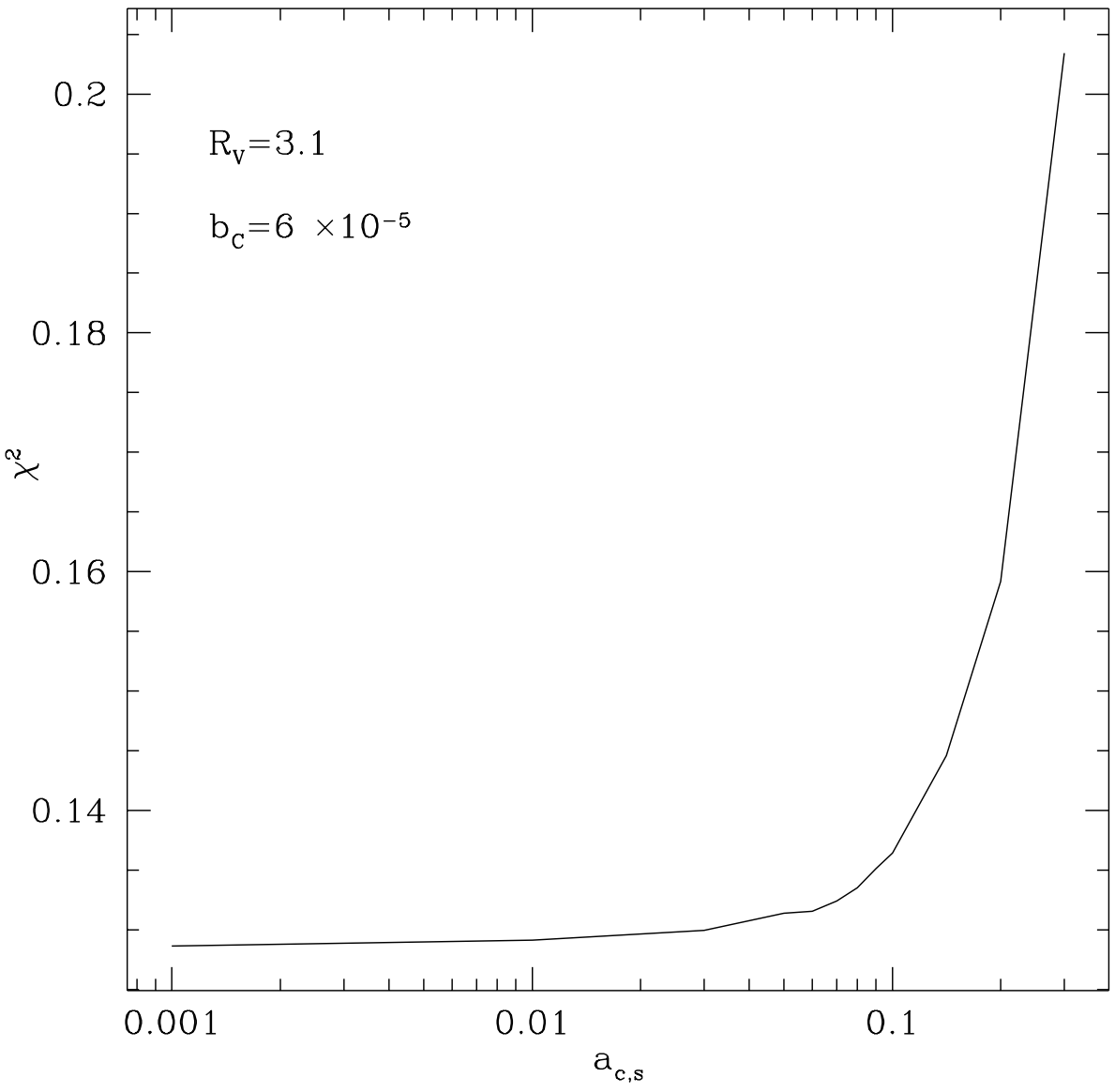


Fig. 1.— The error function $\chi^2$ versus the silicate cutoff parameter, $a_{\rm c,s}$.

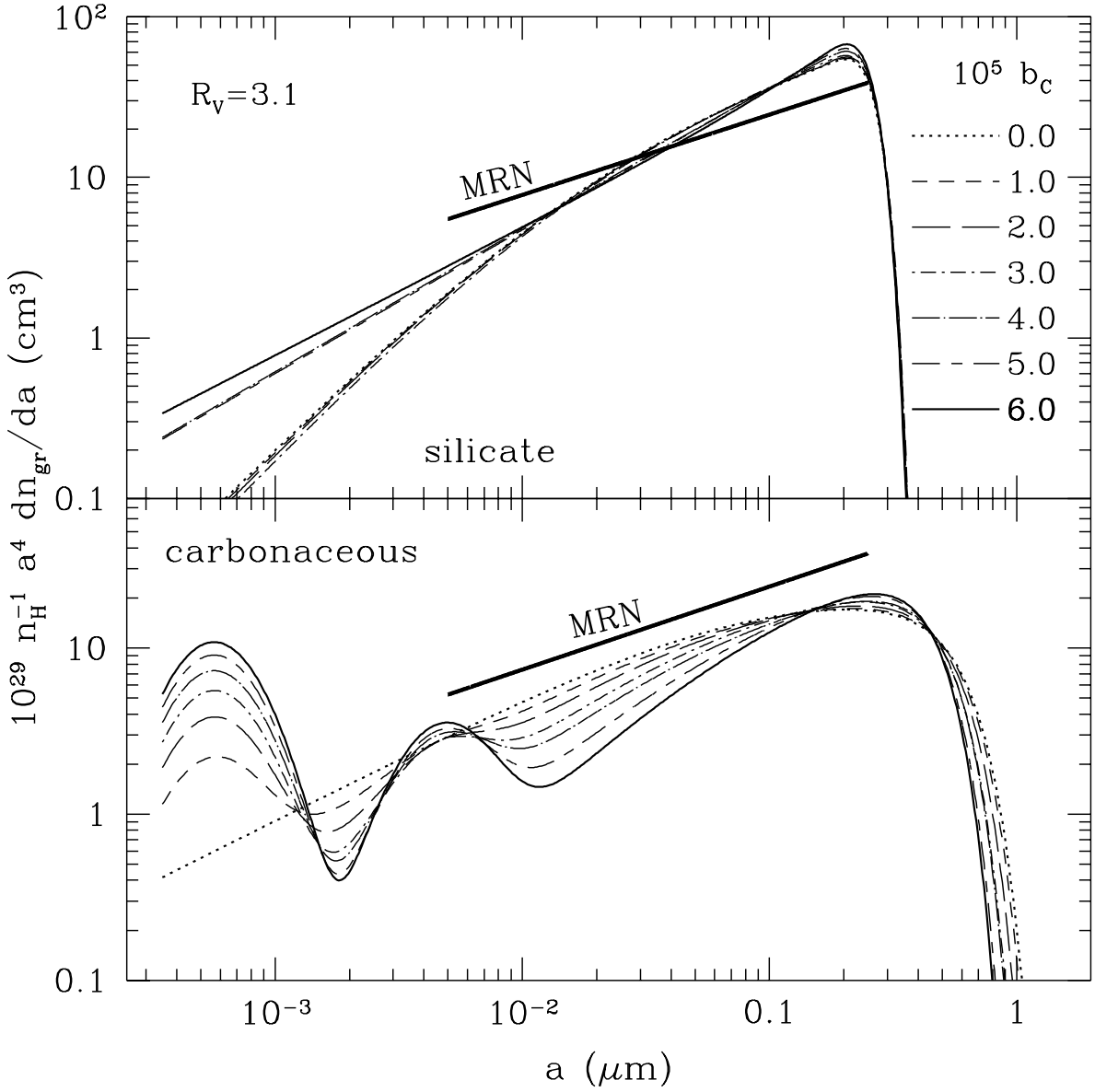


Fig. 2.— Case A grain size distributions for $R_V = 3.1$. The values of $b_C$ are indicated. The heavy, solid lines are the MRN distribution, for comparison. Our favored distribution has $b_C = 6 \times 10^{-5}$ (see text).

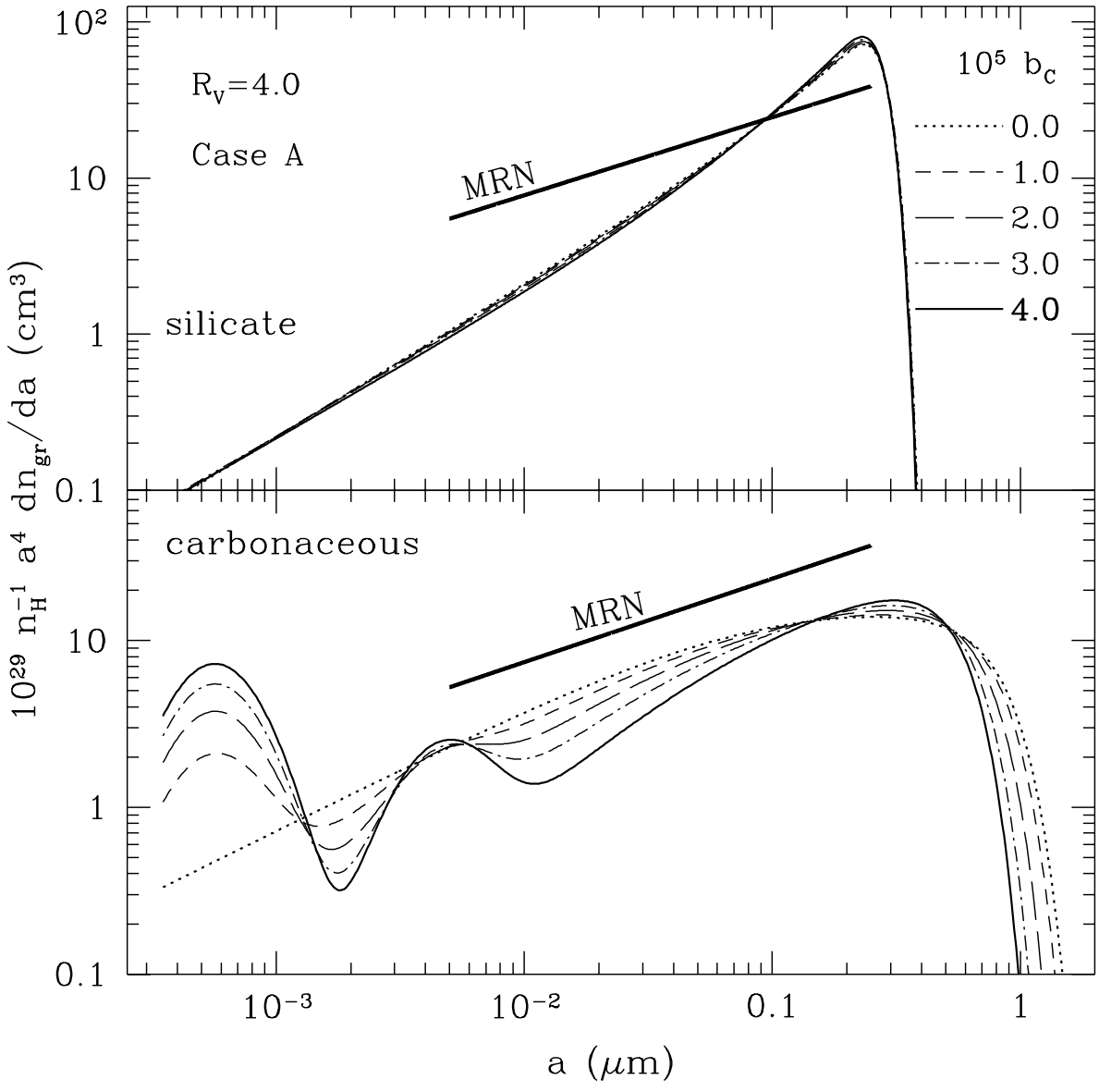


Fig. 3.— Same as Figure 2, but for $R_V = 4.0$. Our favored distribution has $b_C = 4 \times 10^{-5}$ (see text).

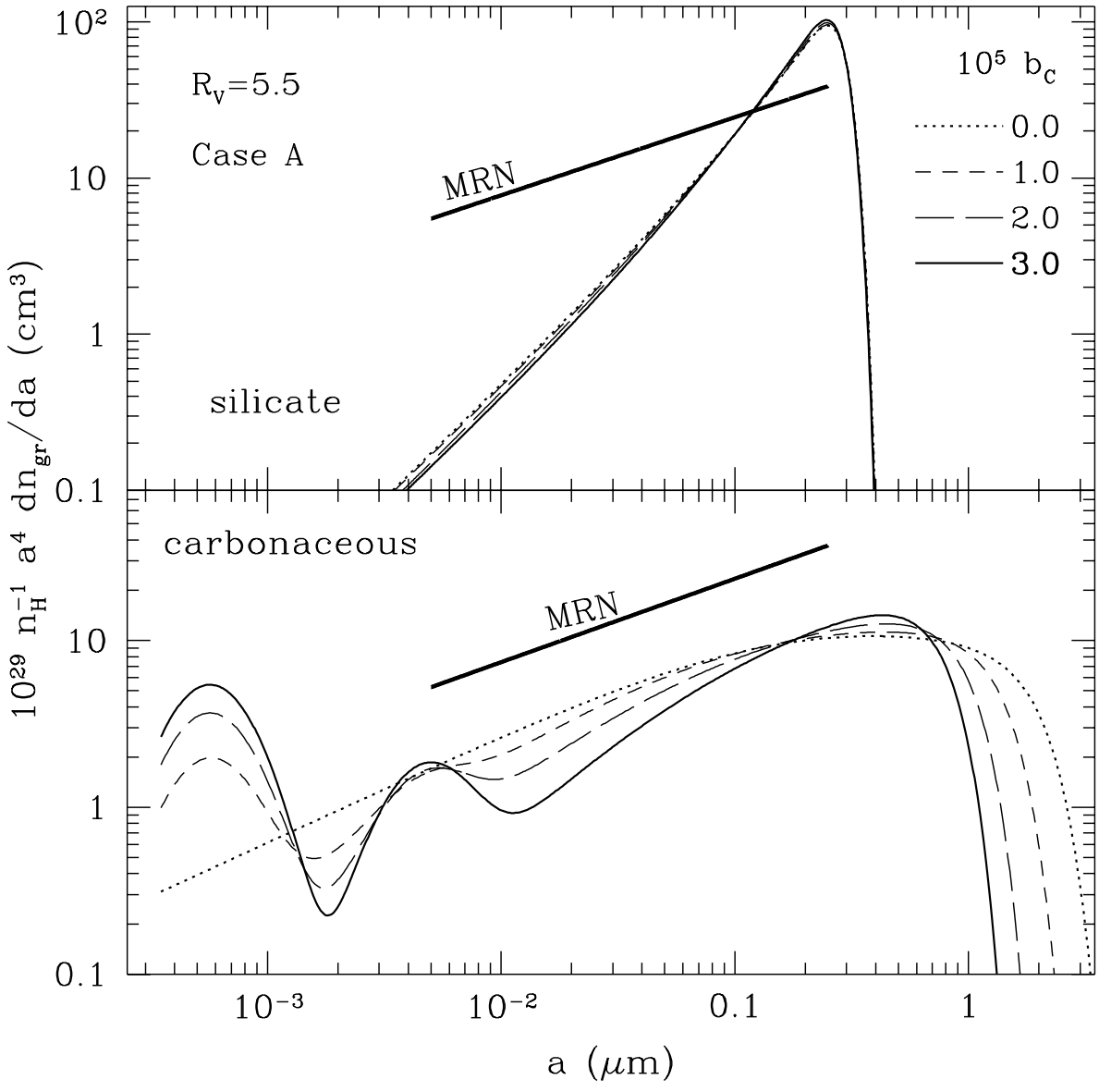


Fig. 4.— Same as Figure 2, but for $R_V = 5.5$. Our favored distribution has $b_C = 3 \times 10^{-5}$ (see text).

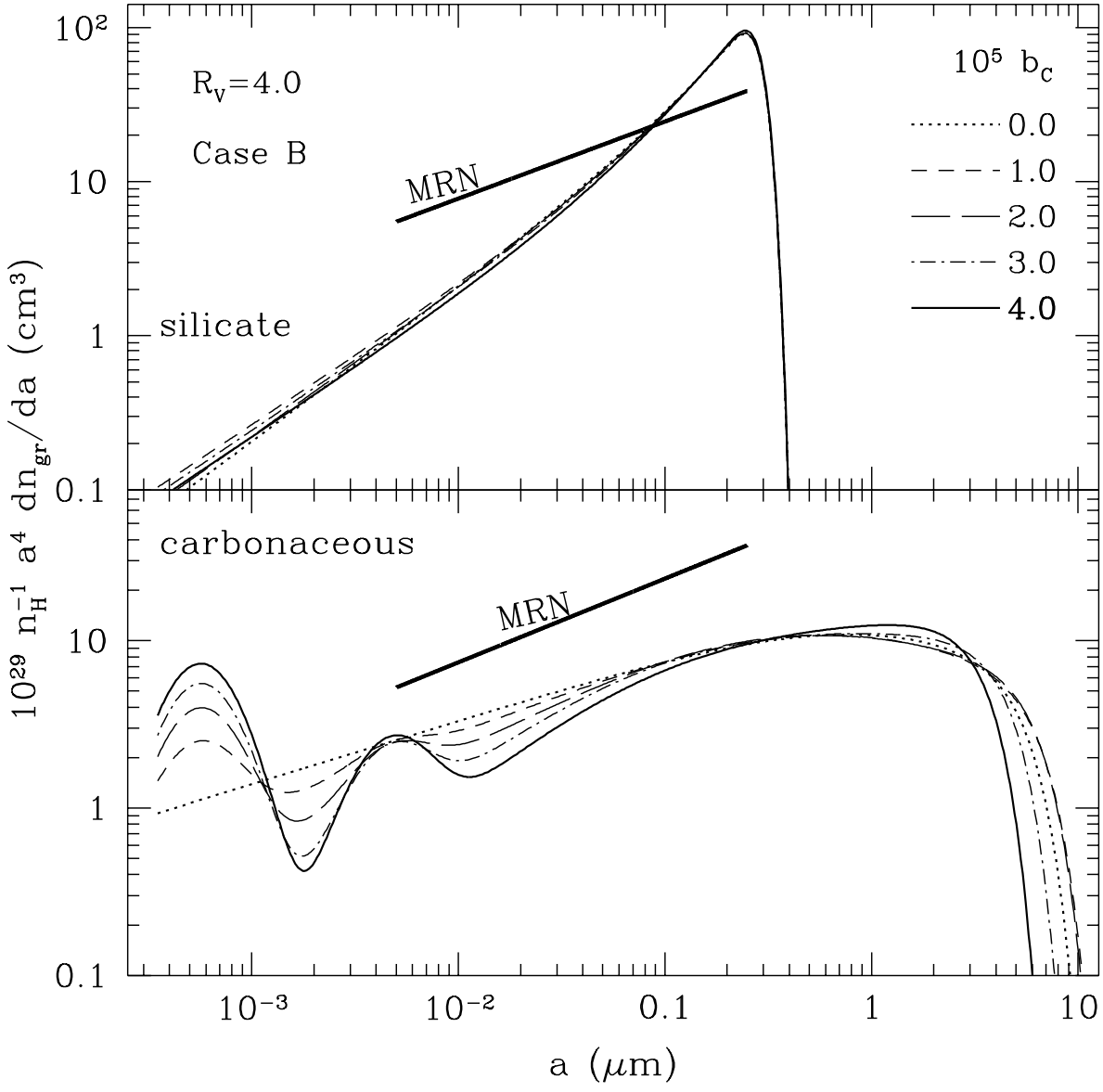


Fig. 5.— Case B size distributions for $R_V = 4.0$.

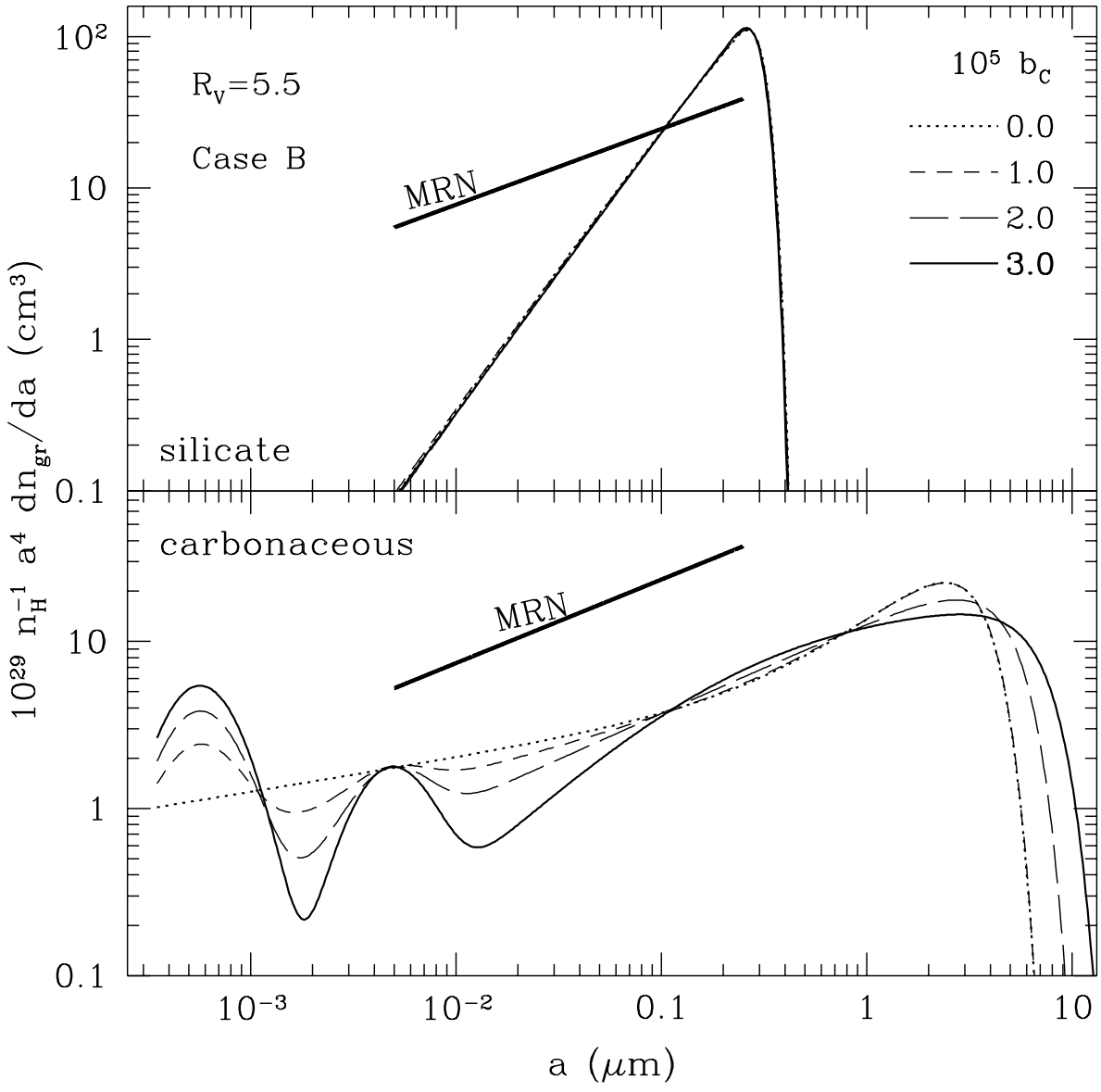


Fig. 6.— Case B size distributions for $R_V = 5.5$.

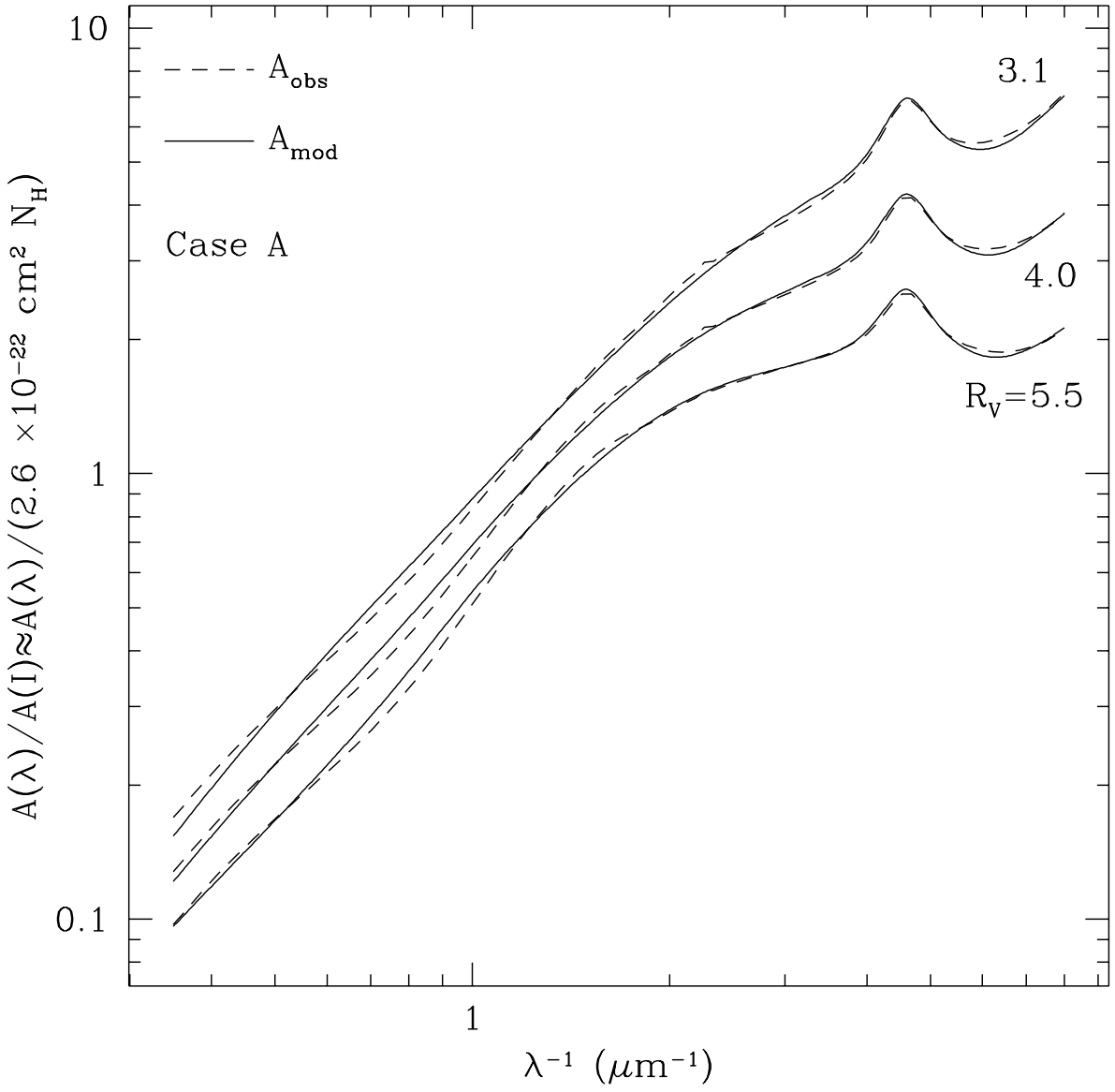


Fig. 7.— The average "observed" extinction $A_{\rm obs}$ and the extinction resulting from our case A models for ($R_V$, $10^5 b_{\rm C}$) = (3.1, 6.0), (4.0, 4.0), and (5.5, 3.0). The curves for $R_V = 4.0$ (5.5) are scaled down by a factor $10^{0.1}$ ($10^{0.2}$), for clarity.

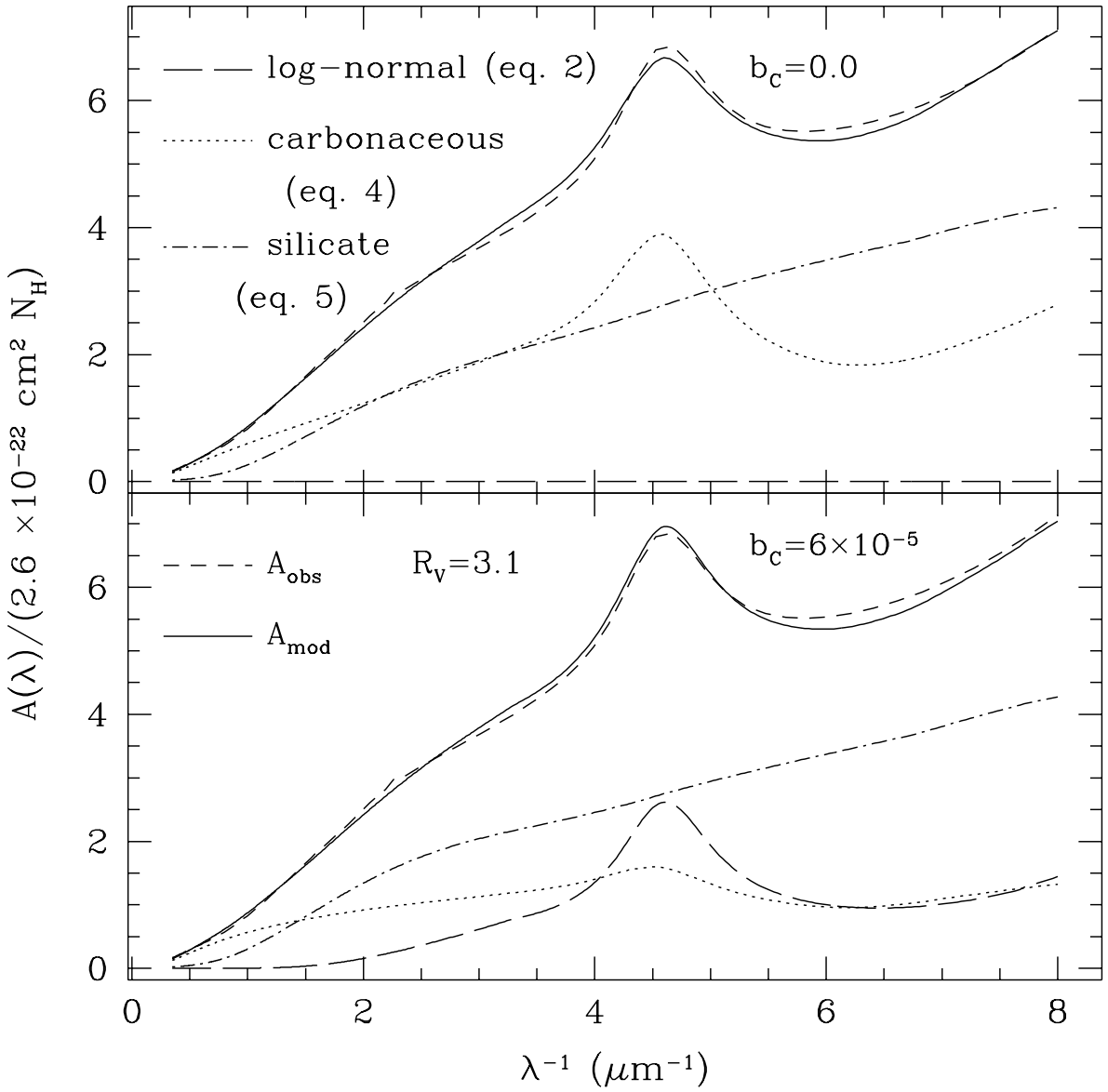


Fig. 8.— The extinction curve $A_{\rm mod}$ resulting from the grain distribution of equations (4) and (5), with parameters optimized to fit $A_{\rm obs}$ (see text) for $R_V = 3.1$ (also shown), for $b_{\rm C} = 0.0$ and $6.0 \times 10^{-5}$. The contributions from the three grain distribution components are also shown.

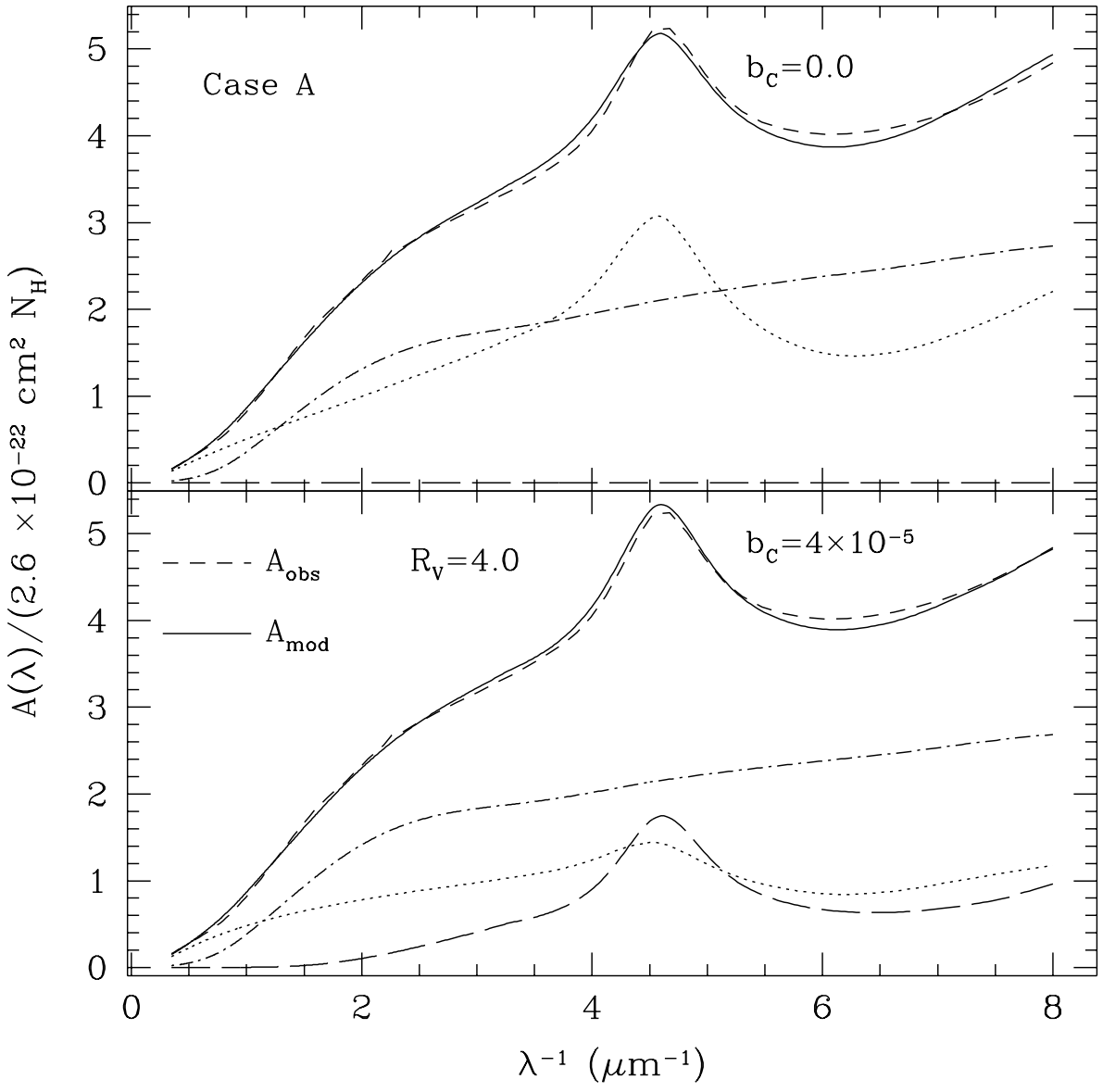


Fig. 9.— Same as Figure 8, but for $R_V = 4.0$ and $b_{\rm C} = 0.0$ and $4.0 \times 10^{-5}$.

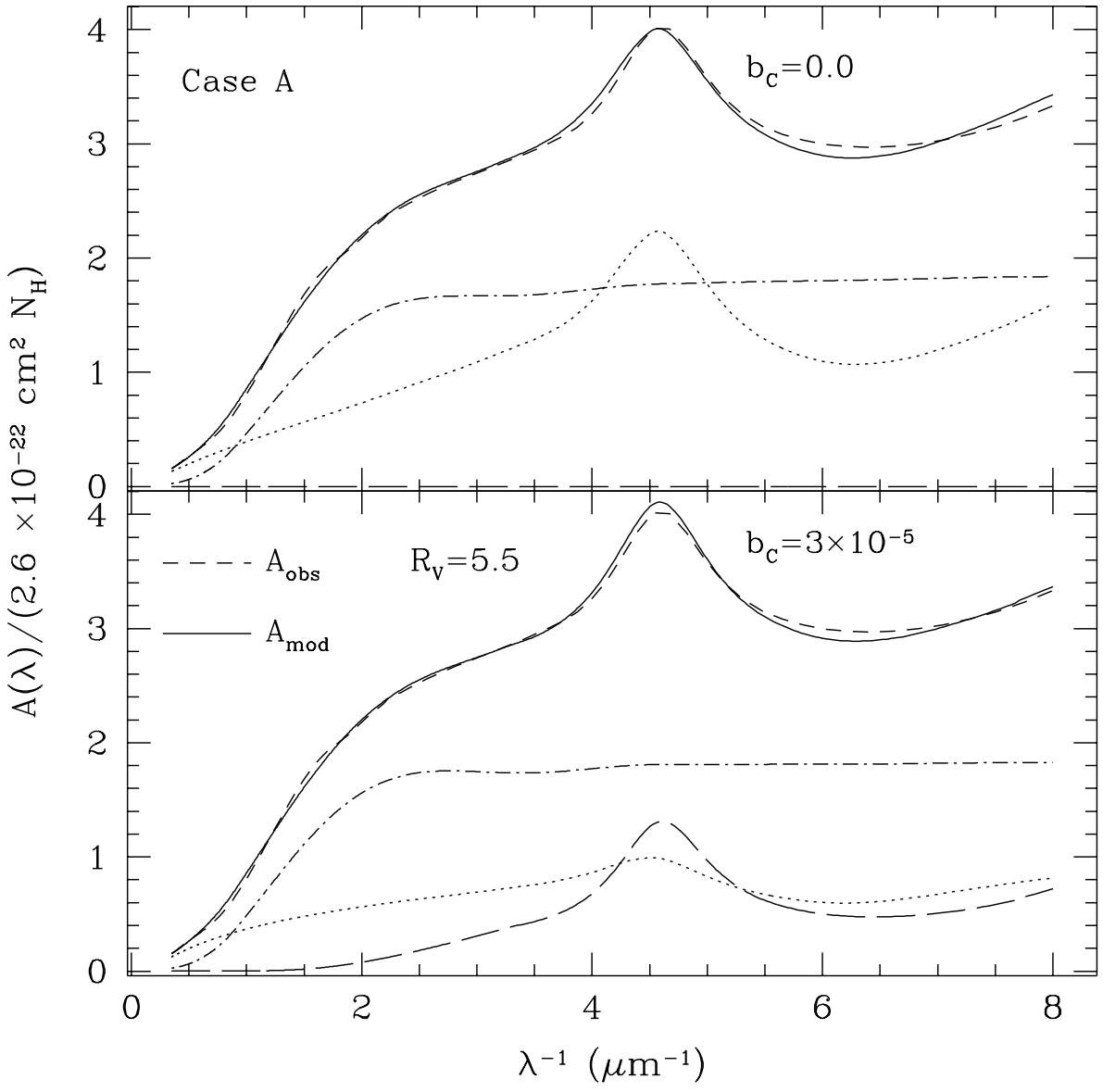


Fig. 10.— Same as Figure 8, but for $R_V = 5.5$ and $b_{\rm C} = 0.0$ and $3.0 \times 10^{-5}$.

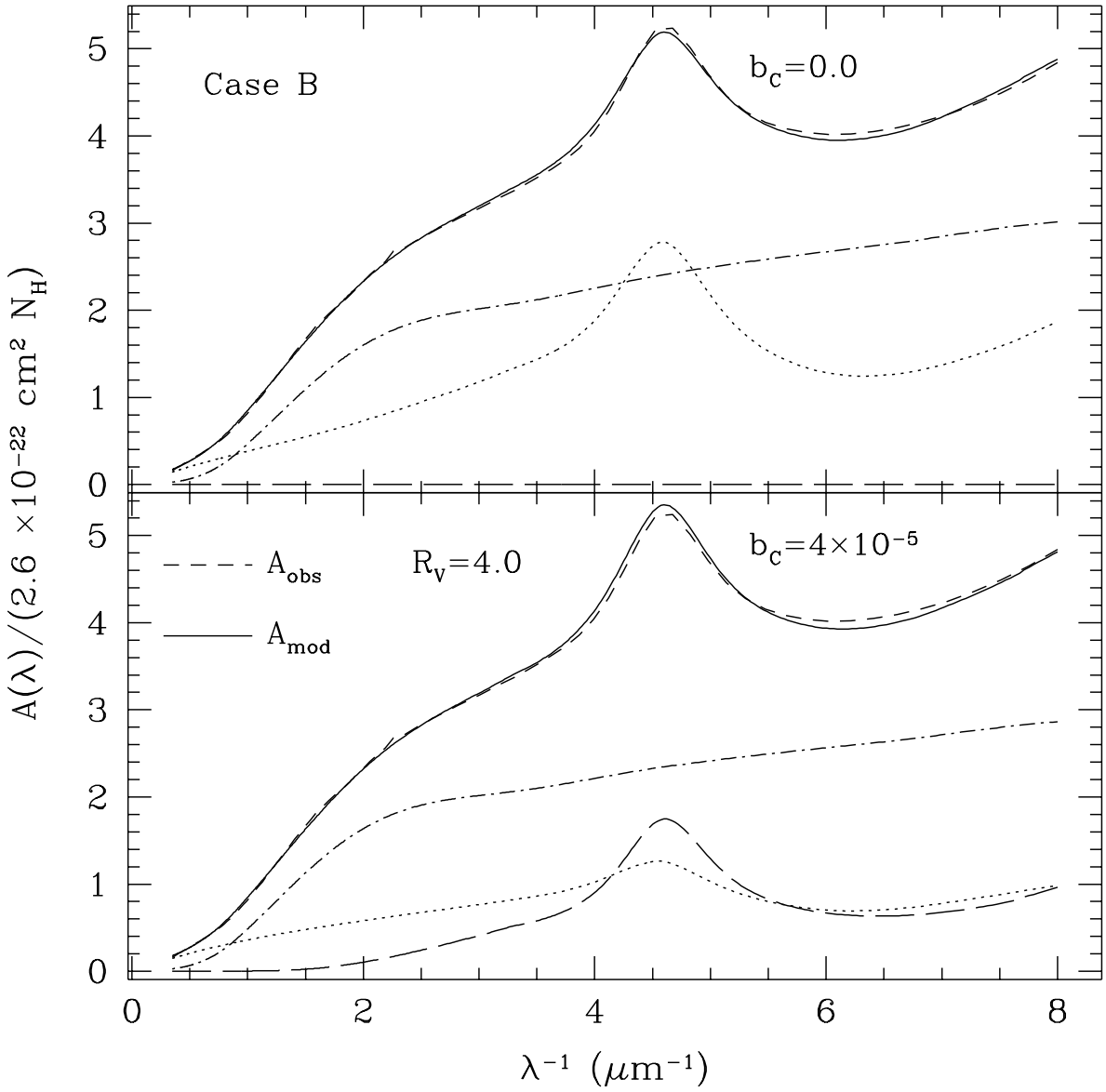


Fig. 11.— Same as Figure 8, but for $R_V = 4.0$, $b_C = 0.0$ and $4.0 \times 10^{-5}$, and fixed total grain volumes $V_{\rm tot,g} = 2.3 \times 10^{-27}\,{\rm cm^3\,H^{-1}}$ and $V_{\rm tot,s} = 3.9 \times 10^{-27}\,{\rm cm^3\,H^{-1}}$.

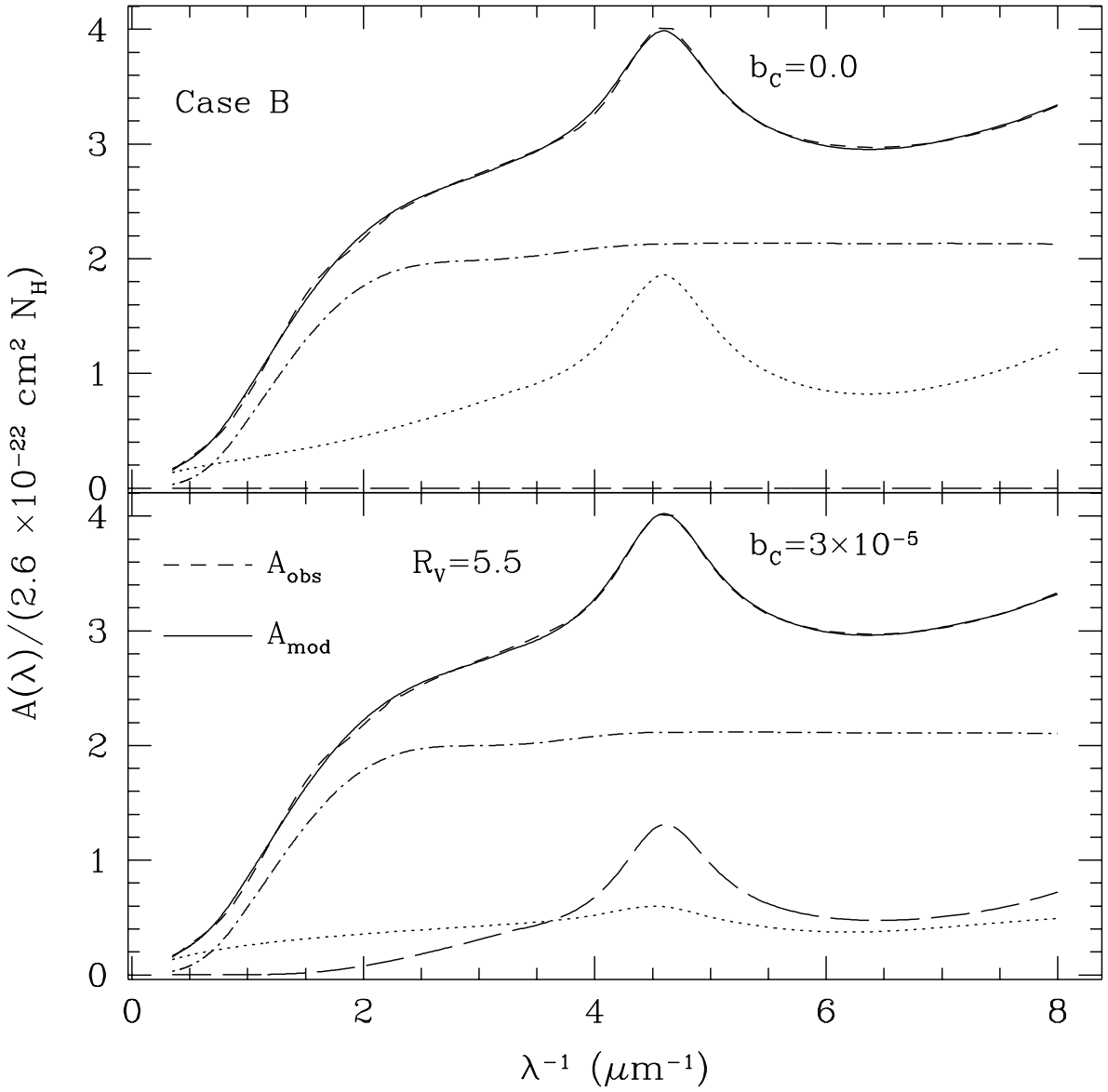


Fig. 12.— Same as Figure 8, but for $R_V = 5.5$, $b_{\rm C} = 0.0$ and $3.0 \times 10^{-5}$, and fixed total grain volumes $V_{\rm tot,g} = 2.3 \times 10^{-27}\,{\rm cm^3\,H^{-1}}$ and $V_{\rm tot,s} = 3.9 \times 10^{-27}\,{\rm cm^3\,H^{-1}}$.

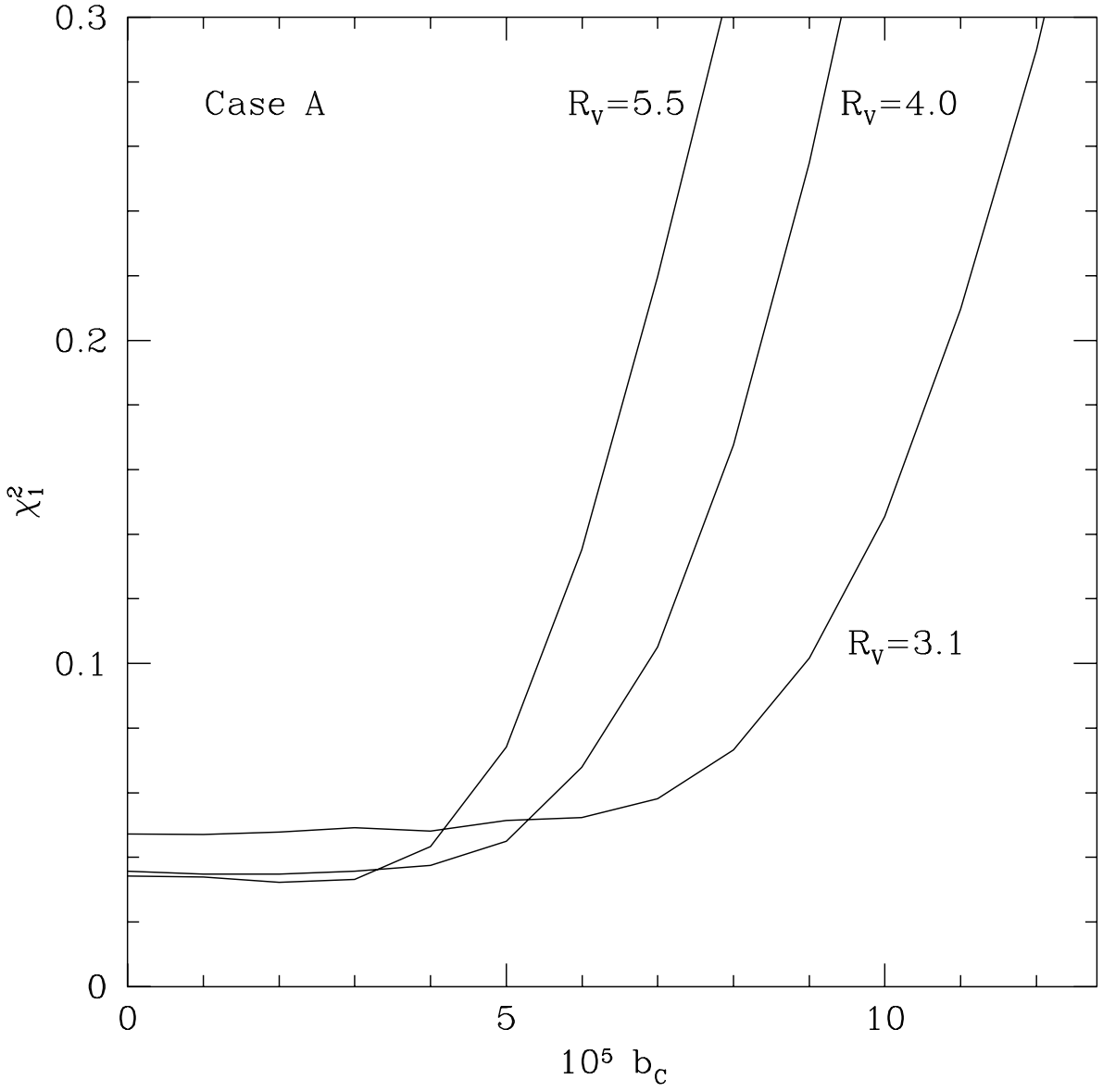


Fig. 13.— The extinction fit error function $\chi_1^2$ (§2.5) as a function of $b_{\rm C}$, the C abundance in the log-normal grain population, for three values of $R_V$.

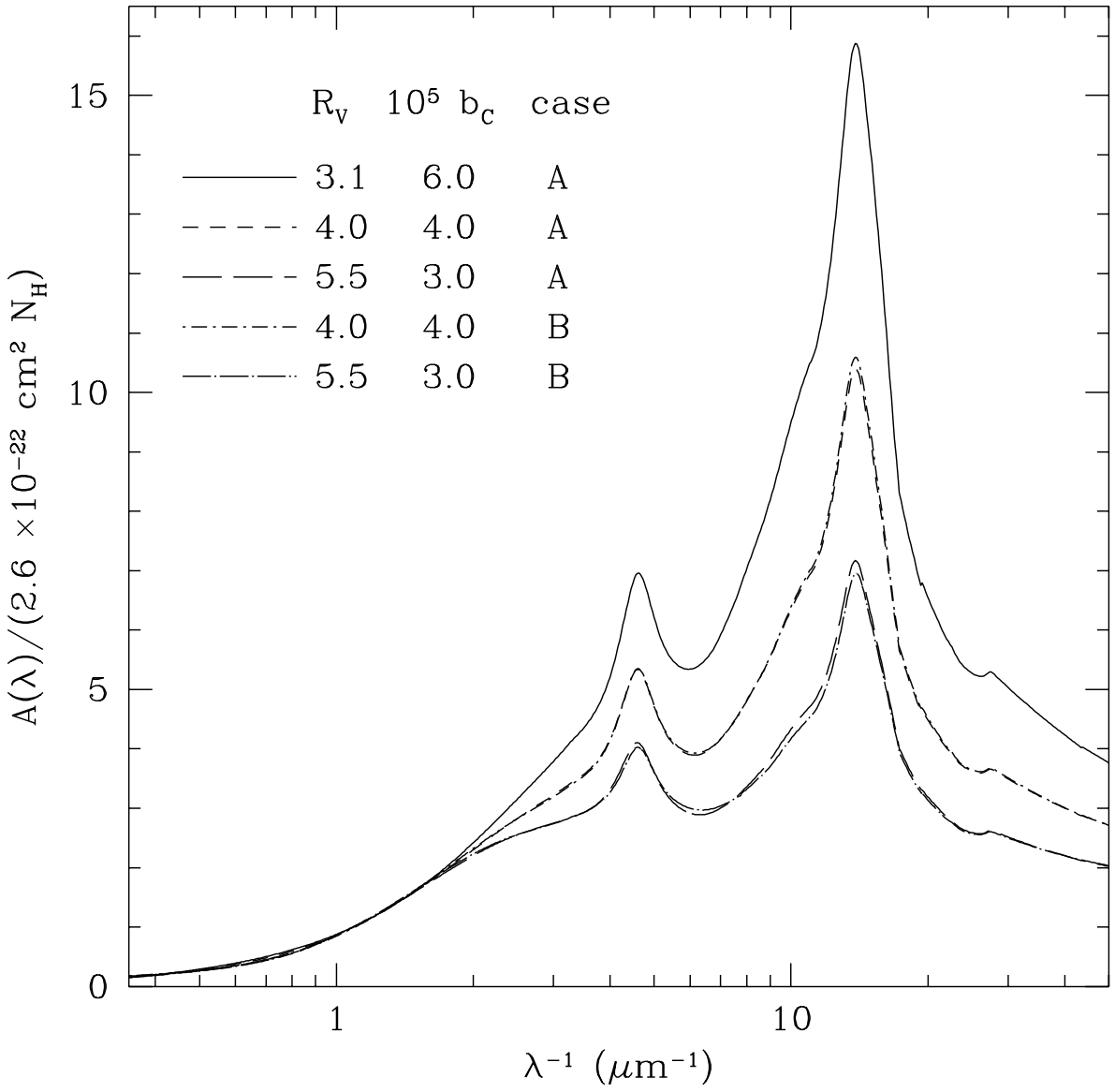


Fig. 14.— Model extinction curves extended to short wavelengths, for various size distributions.

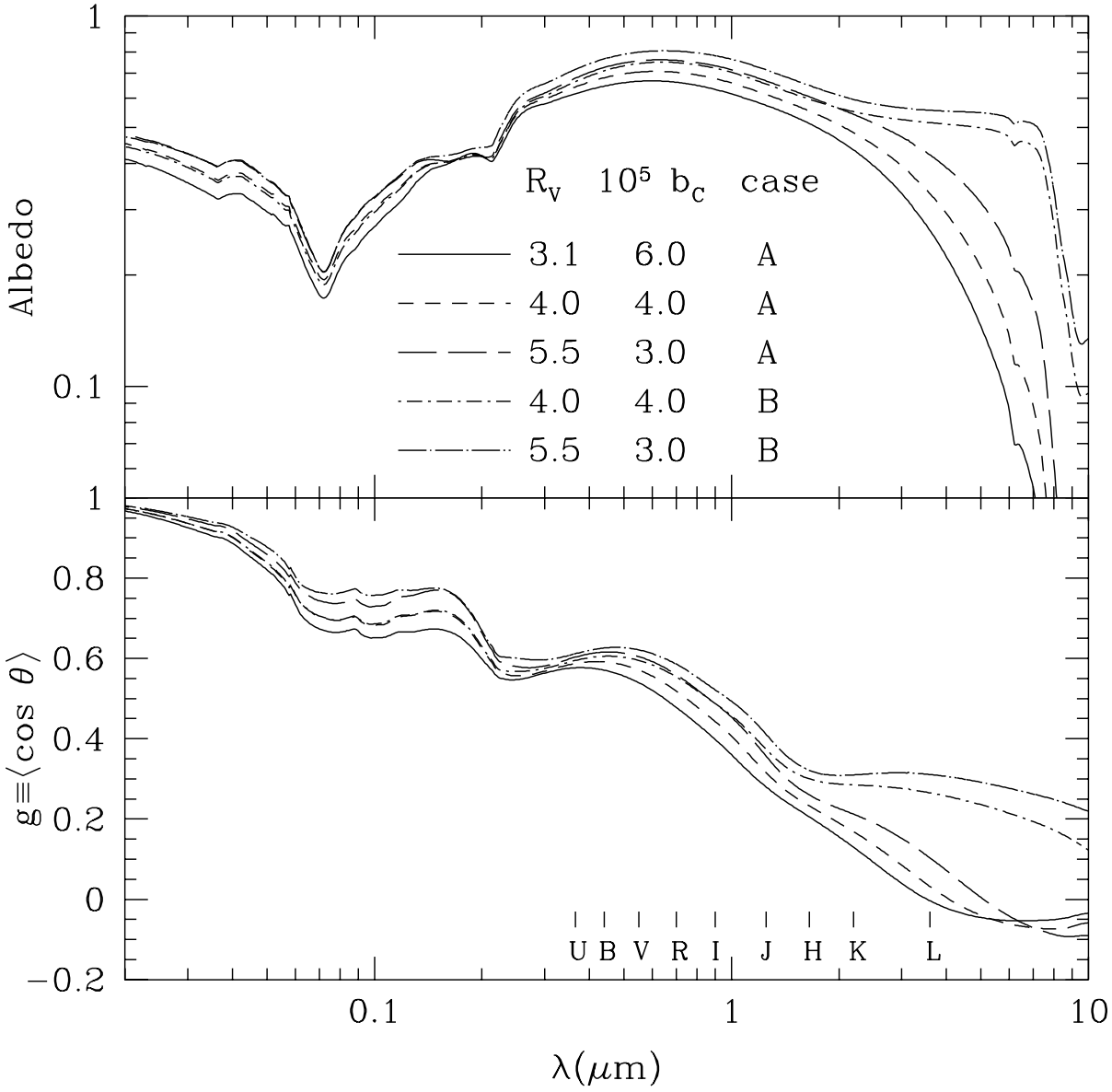


Fig. 15.— Albedo and asymmetry parameter $g \equiv \langle \cos\theta \rangle$ for various size distributions.

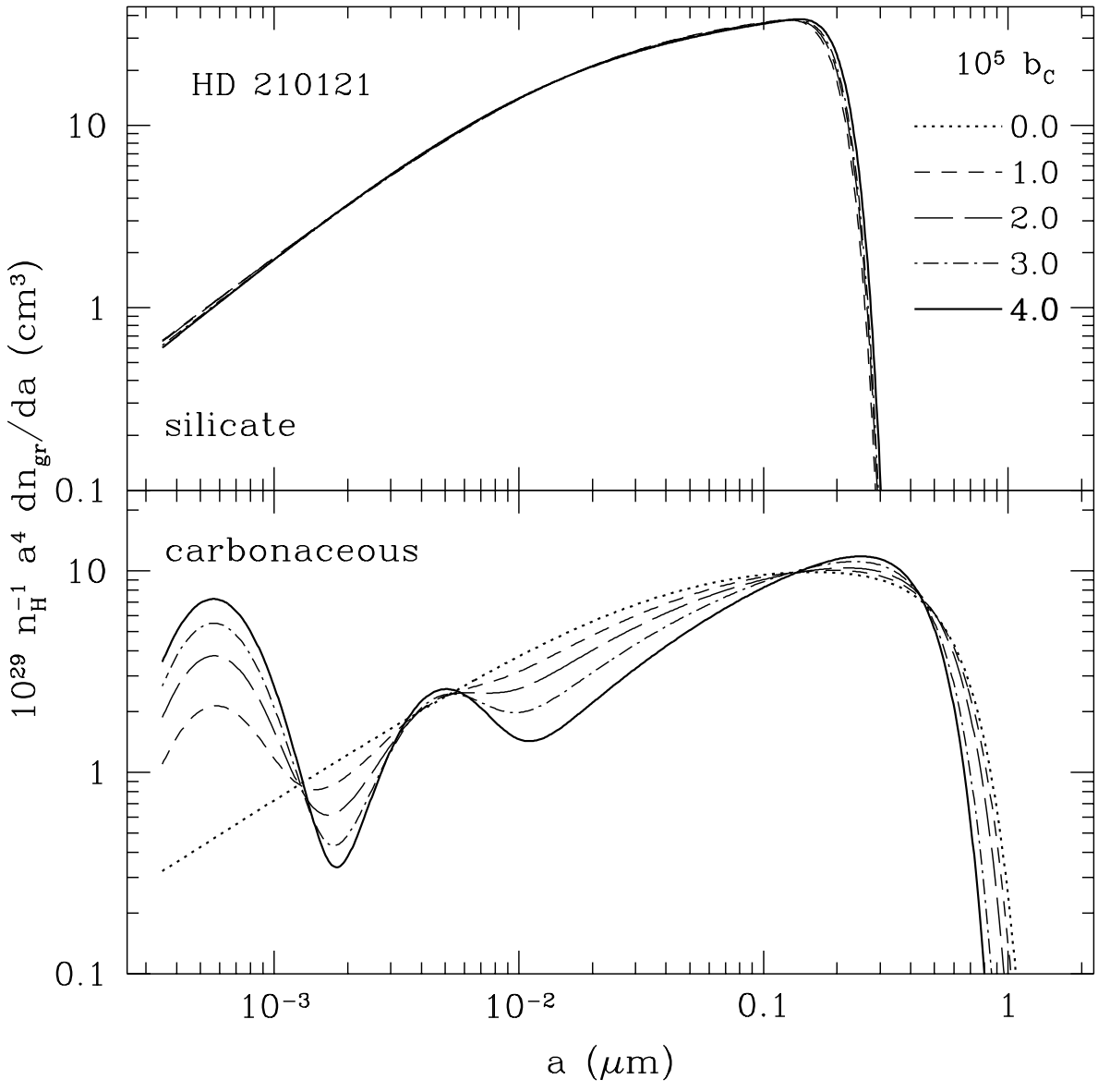


Fig. 16.— Grain size distributions for HD 210121.

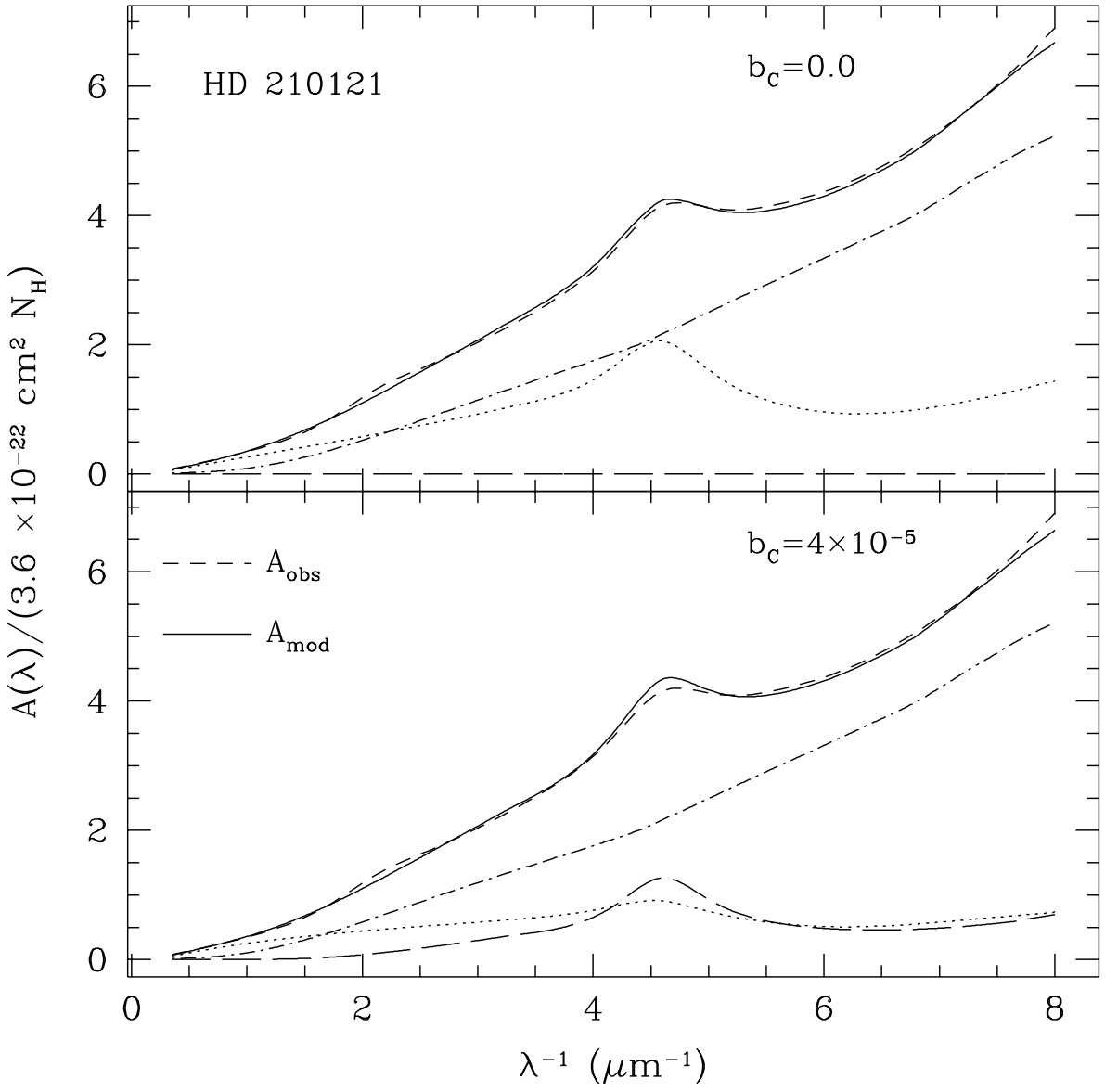


Fig. 17.— Same as Figure 8, but for the extinction along the line of sight to HD 210121 and $b_{\rm C} = 0.0$ and $4.0 \times 10^{-5}$. Note the difference in vertical scale from Figure 8.

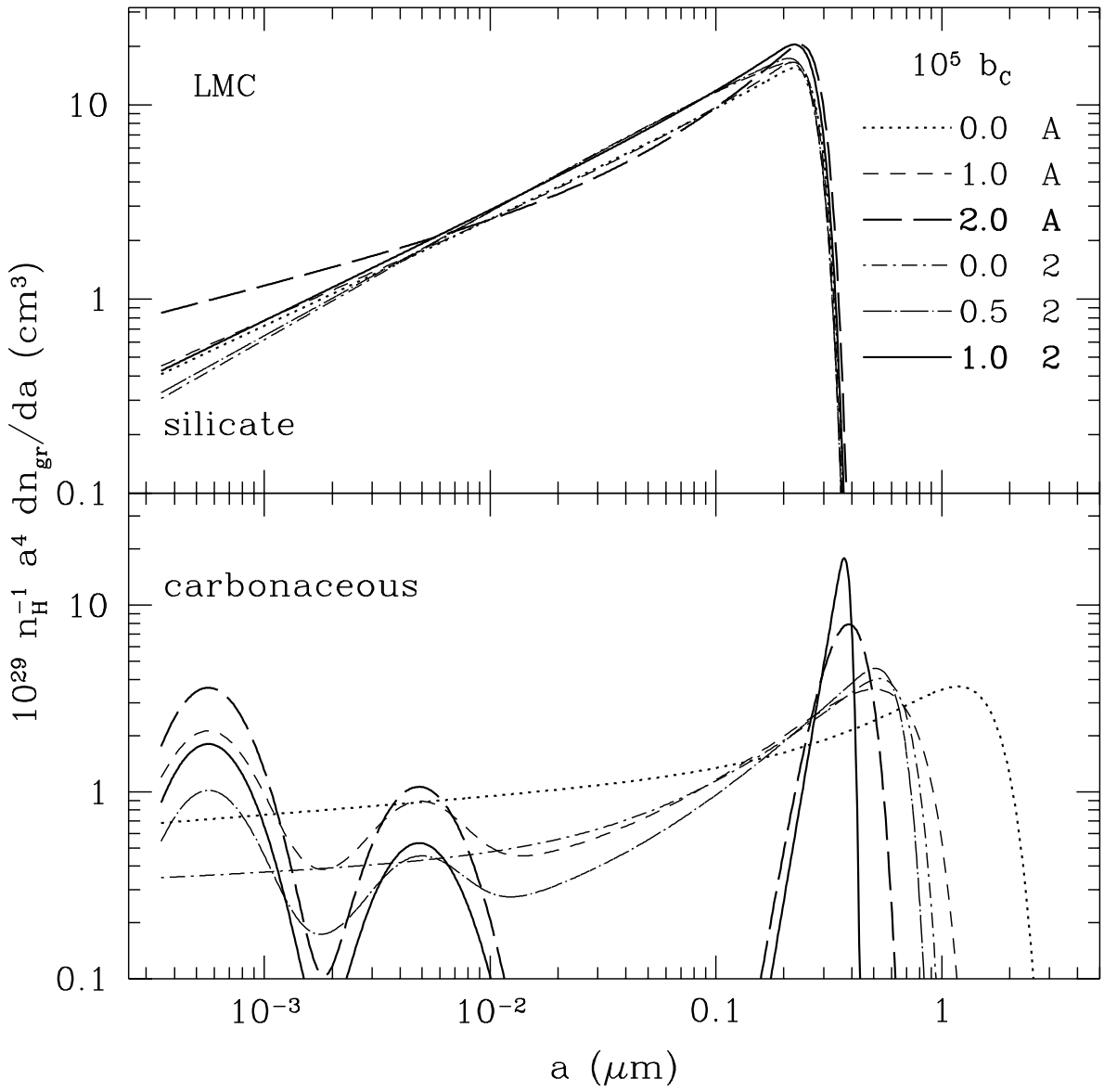


Fig. 18.— Grain size distributions for the LMC. The values of $b_C$ are indicated; "A" denotes distributions constructed to fit the average extinction in the LMC and "2"denotes distributions for the LMC 2 area.

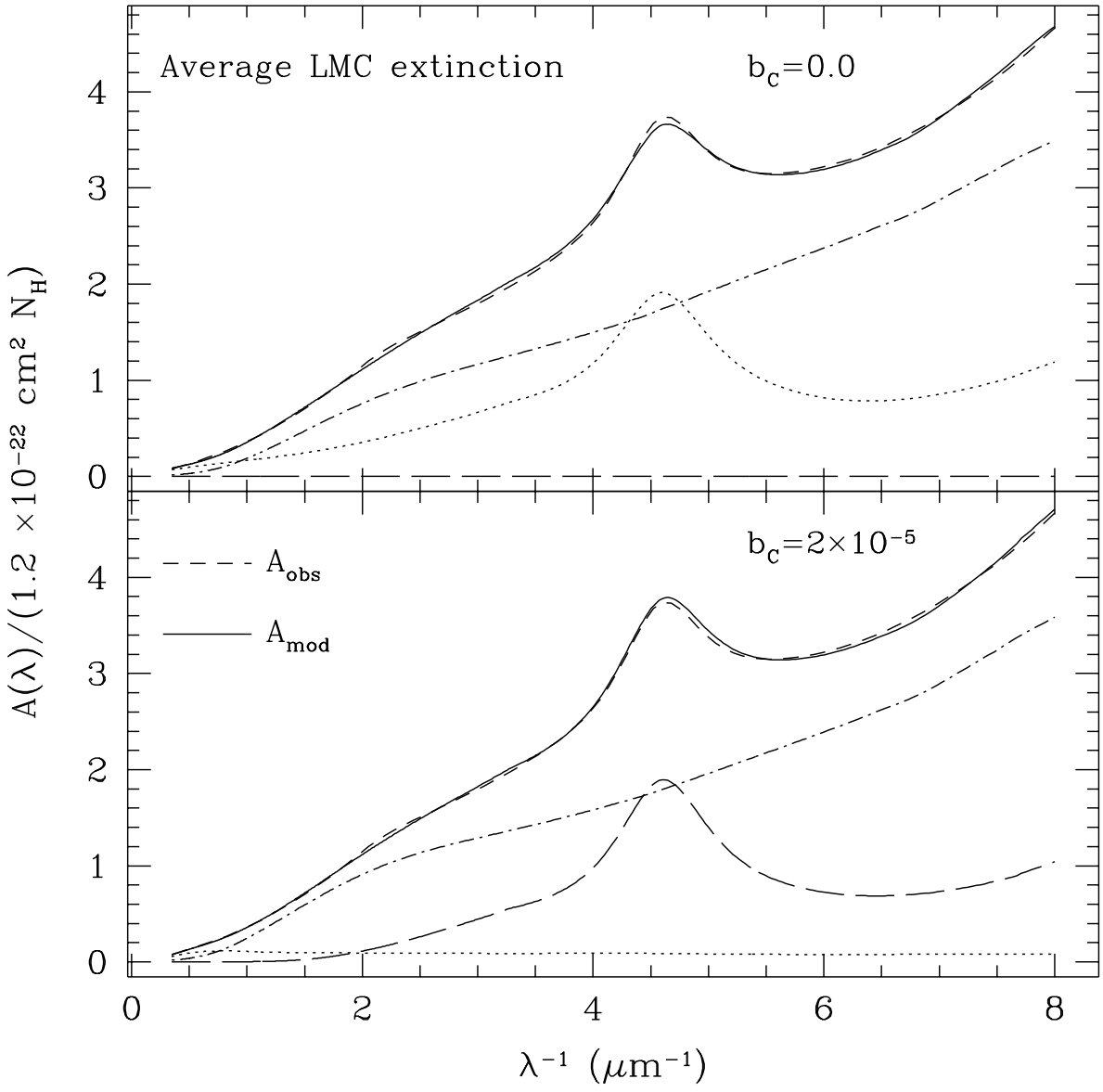


Fig. 19.— Same as Figure 8, but for the average extinction for the LMC and $b_{\rm C} = 0.0$ and $2.0\times10^{-5}$. Note the difference in vertical scale from Figure 8.

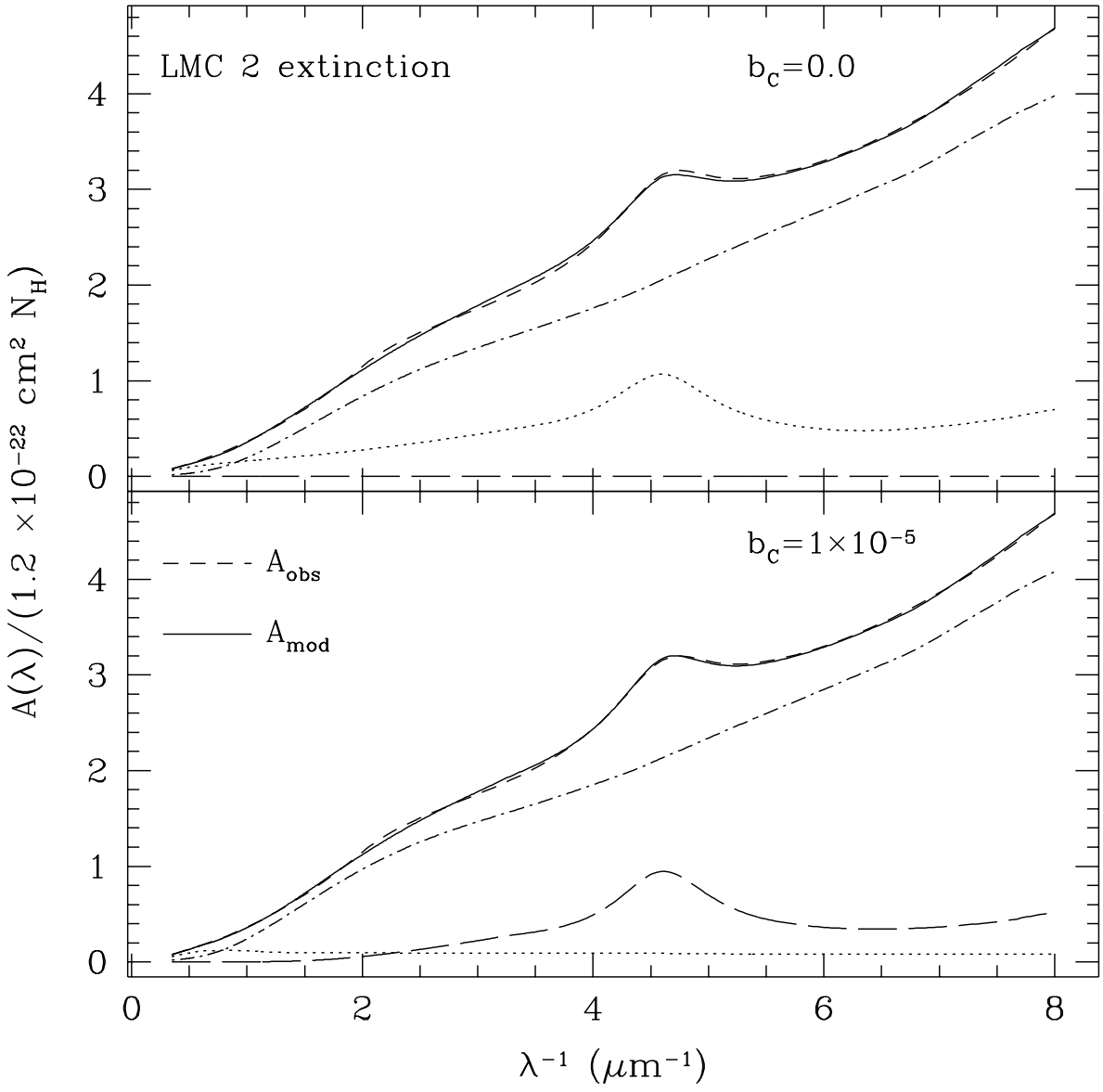


Fig. 20.— Same as Figure 8, but for the LMC 2 area and $b_{\rm C} = 0.0$ and $1.0 \times 10^{-5}$. Note the difference in vertical scale from Figure 8.

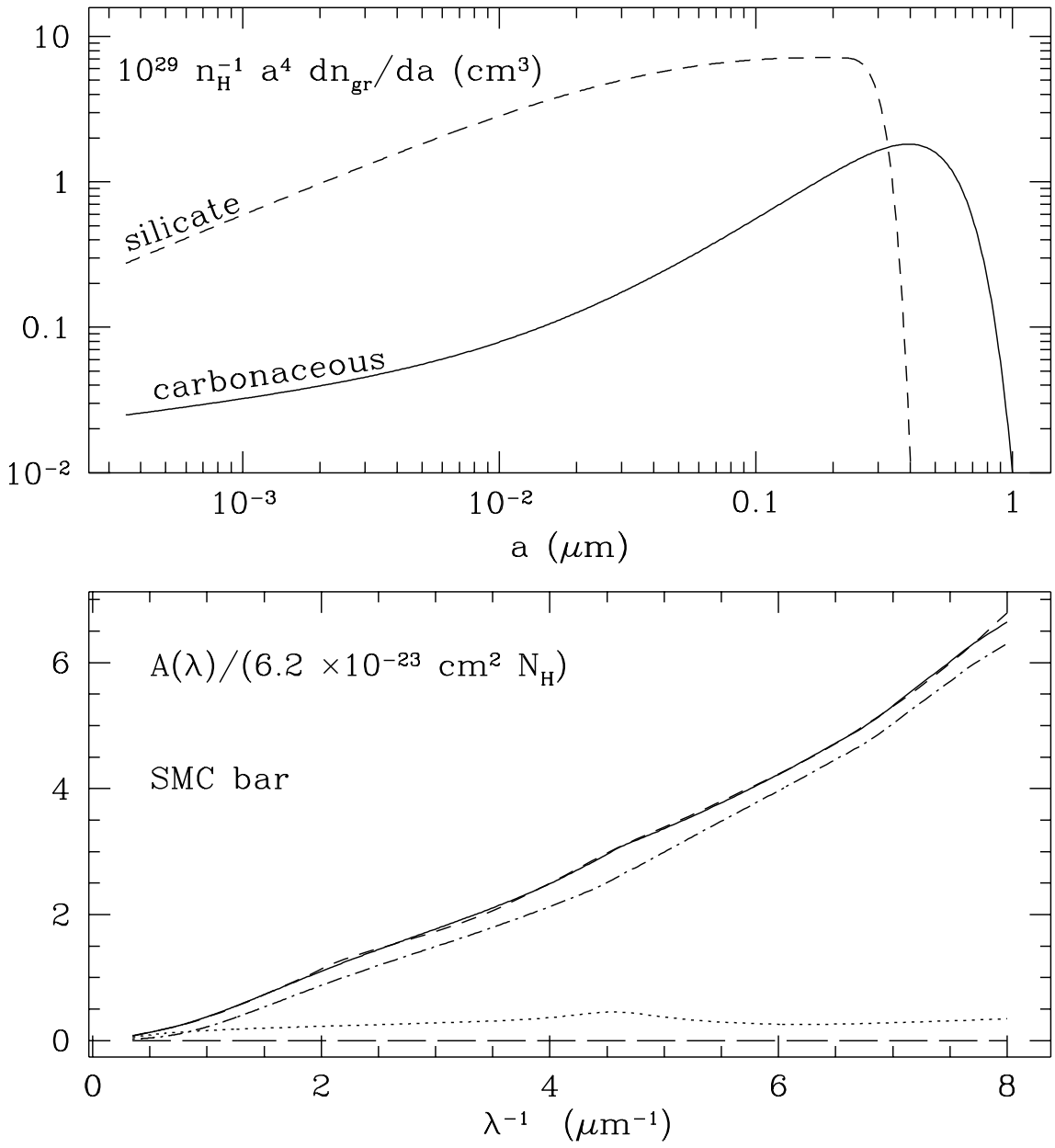


Fig. 21.— Upper panel: Size distribution for the SMC bar, with $b_C = 0.0$. Lower panel: The corresponding extinction fit; curve types are the same as in Figure 8.

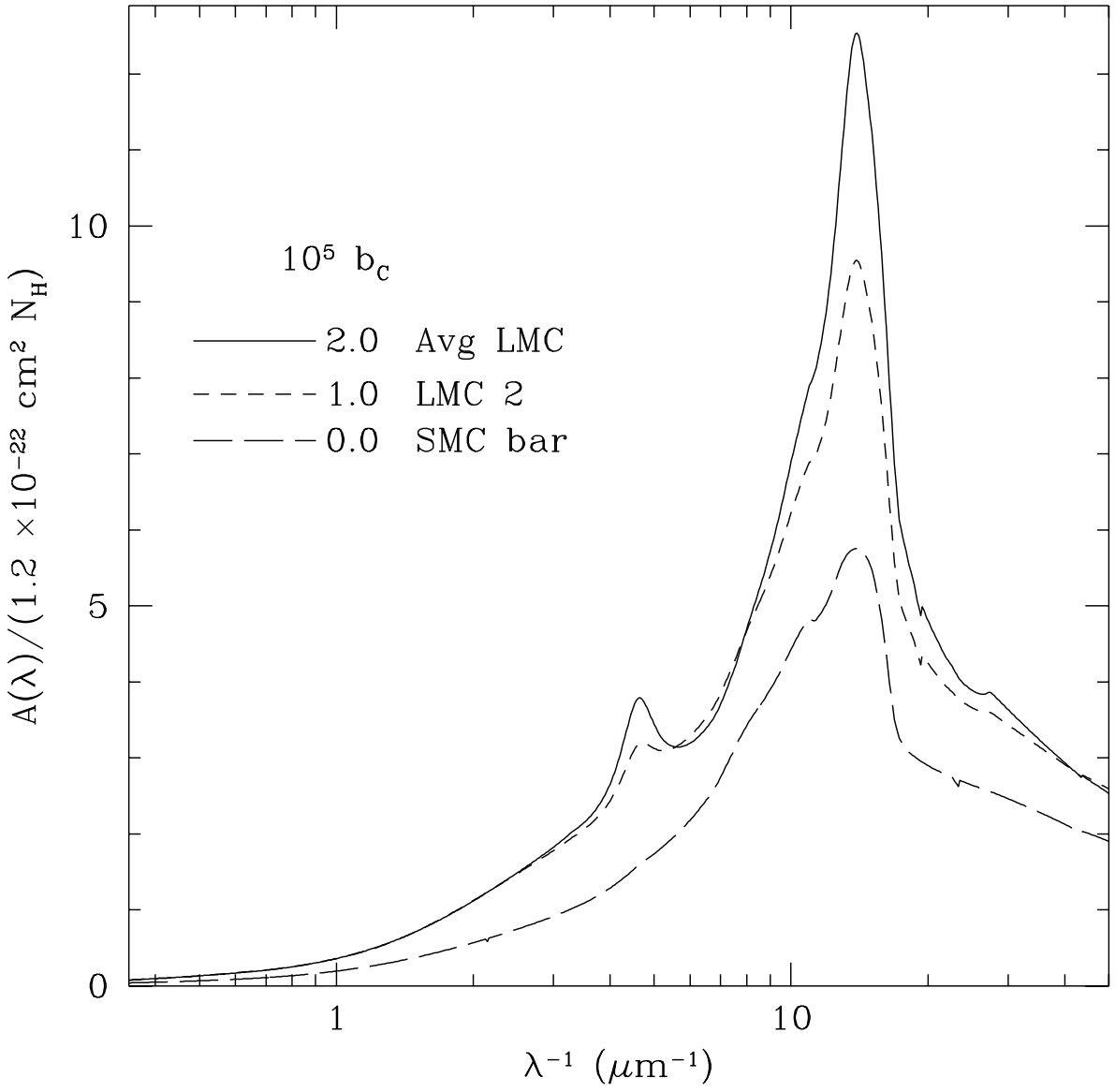


Fig. 22.— Model extinction curves extended to short wavelengths, for Magellanic Cloud environments.

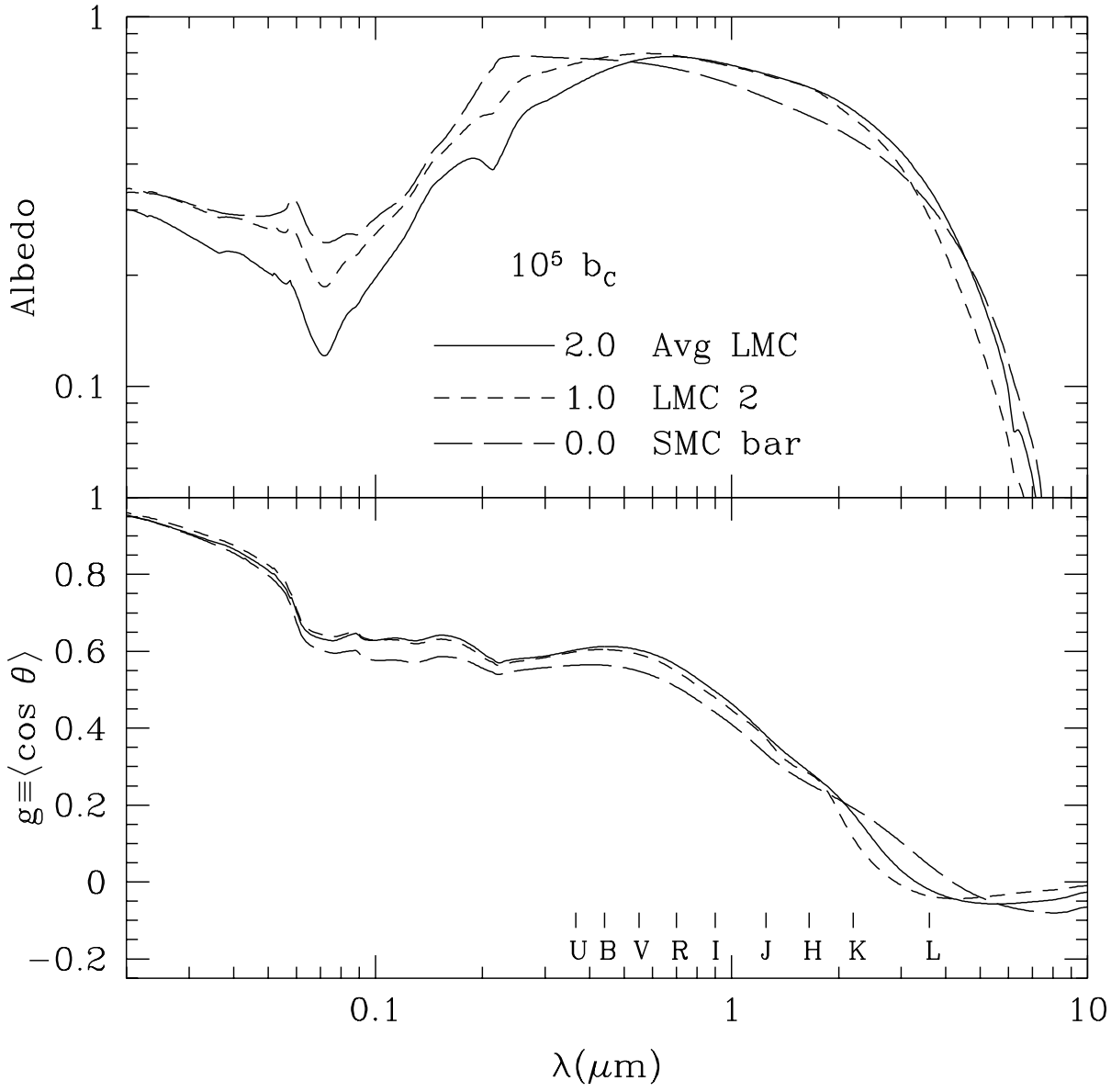


Fig. 23.— Albedo and asymmetry parameter $g \equiv \langle \cos\theta \rangle$ for Magellanic Cloud environments.

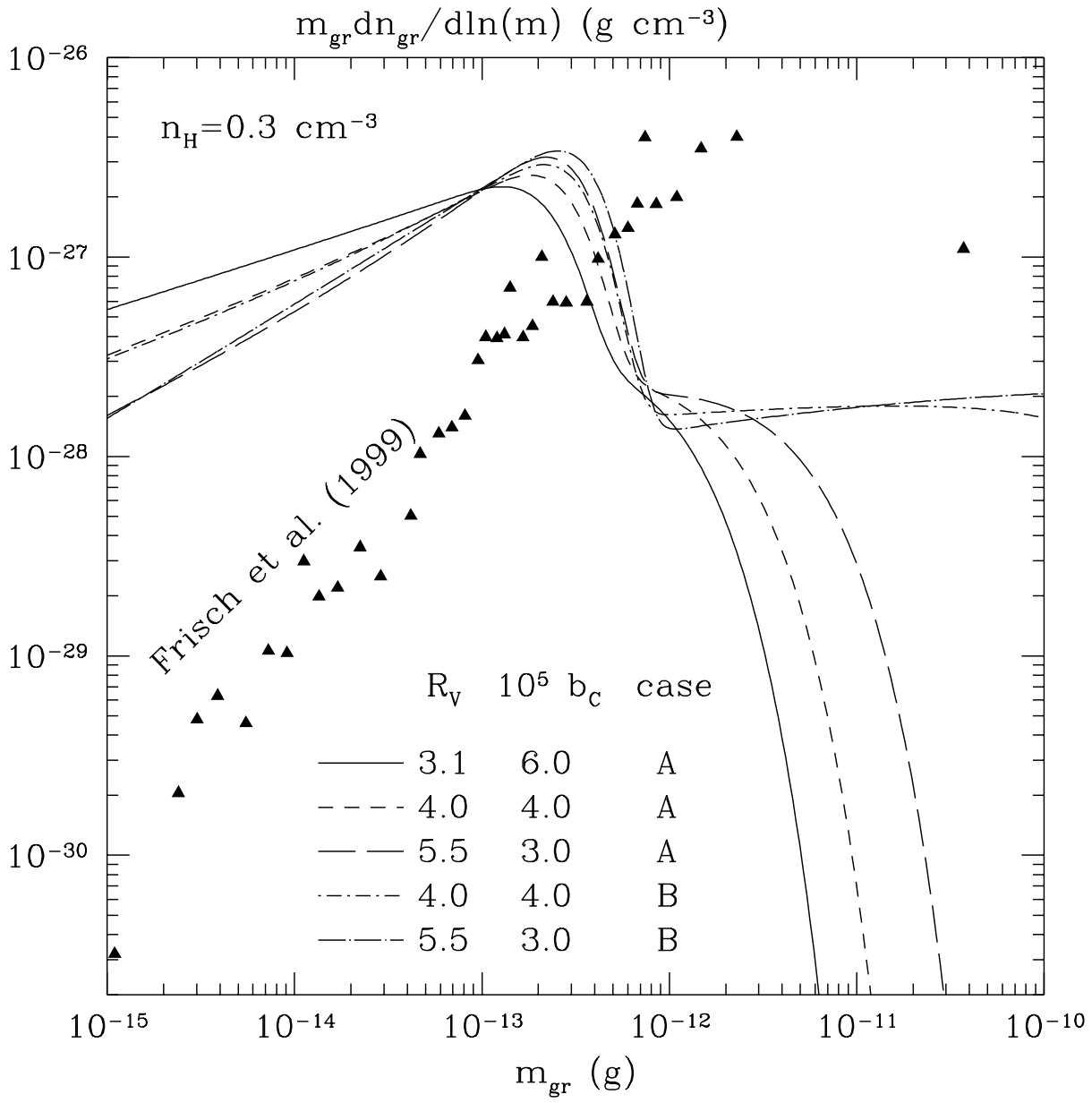


Fig. 24.— Mass distribution for grains in the local ISM determined by Frisch et al. (1999) (triangles). Mass distributions for the size distributions of §3 are also shown; the sharp drop at $m \sim 3 \times 10^{-13}$ g corresponds to the rapid drop in silicate grain abundance at $a \sim 0.3\mu$m.

Table 1. Grain Size Distribution Parameter Values[a]

| $R_V$[b] | $10^5 b_C$[c] | case | $\alpha_g$ | $\beta_g$ | $a_{t,g}$ ($\mu$m) | $a_{c,g}$ ($\mu$m) | $C_g$ | $\alpha_s$ | $\beta_s$ | $a_{t,s}$ ($\mu$m) | $C_s$ | $\tilde{V}_g$[d] | $\tilde{V}_s$[d] | $\chi^2_1$[e] | $\chi^2_2$[f] | $\chi^2$[g] |
|---|---|---|---|---|---|---|---|---|---|---|---|---|---|---|---|---|
| 3.1 | 0.0 | A | -2.25 | -0.0648 | 0.00745 | 0.606 | $9.94 \times 10^{-11}$ | -1.48 | -9.34 | 0.172 | $1.02 \times 10^{-12}$ | 1.146 | 1.244 | 0.047 | 0.111 | 0.118 |
| 3.1 | 1.0 | A | -2.17 | -0.0382 | 0.00373 | 0.586 | $3.79 \times 10^{-10}$ | -1.46 | -10.3 | 0.174 | $1.09 \times 10^{-12}$ | 1.137 | 1.251 | 0.047 | 0.116 | 0.118 |
| 3.1 | 2.0 | A | -2.04 | -0.111 | 0.00828 | 0.543 | $5.57 \times 10^{-11}$ | -1.43 | -11.7 | 0.173 | $1.27 \times 10^{-12}$ | 1.130 | 1.254 | 0.048 | 0.124 | 0.118 |
| 3.1 | 3.0 | A | -1.91 | -0.125 | 0.00837 | 0.499 | $4.15 \times 10^{-11}$ | -1.41 | -11.5 | 0.171 | $1.33 \times 10^{-12}$ | 1.119 | 1.260 | 0.049 | 0.139 | 0.119 |
| 3.1 | 4.0 | A | -1.84 | -0.132 | 0.00898 | 0.489 | $2.90 \times 10^{-11}$ | -2.10 | -0.114 | 0.169 | $1.26 \times 10^{-13}$ | 1.113 | 1.290 | 0.048 | 0.135 | 0.126 |
| 3.1 | 5.0 | A | -1.72 | -0.322 | 0.0254 | 0.438 | $3.20 \times 10^{-12}$ | -2.10 | -0.0407 | 0.166 | $1.27 \times 10^{-13}$ | 1.098 | 1.304 | 0.051 | 0.154 | 0.131 |
| 3.1 | 6.0 | A | -1.54 | -0.165 | 0.0107 | 0.428 | $9.99 \times 10^{-12}$ | -2.21 | 0.300 | 0.164 | $1.00 \times 10^{-13}$ | 1.092 | 1.322 | 0.052 | 0.161 | 0.136 |
| 4.0 | 0.0 | A | -2.26 | -0.199 | 0.0241 | 0.861 | $5.47 \times 10^{-12}$ | -2.03 | 0.668 | 0.189 | $5.20 \times 10^{-14}$ | 1.000 | 1.100 | 0.036 | 0.100 | 0.048 |
| 4.0 | 1.0 | A | -2.16 | -0.0862 | 0.00867 | 0.803 | $4.58 \times 10^{-11}$ | -2.05 | 0.832 | 0.188 | $4.81 \times 10^{-14}$ | 0.992 | 1.103 | 0.035 | 0.104 | 0.048 |
| 4.0 | 2.0 | A | -2.01 | -0.0973 | 0.00811 | 0.696 | $3.96 \times 10^{-11}$ | -2.06 | 0.995 | 0.185 | $4.70 \times 10^{-14}$ | 0.974 | 1.112 | 0.035 | 0.113 | 0.050 |
| 4.0 | 3.0 | A | -1.83 | -0.175 | 0.0117 | 0.604 | $1.42 \times 10^{-11}$ | -2.08 | 1.29 | 0.184 | $4.26 \times 10^{-14}$ | 0.957 | 1.121 | 0.036 | 0.130 | 0.053 |
| 4.0 | 4.0 | A | -1.64 | -0.247 | 0.0152 | 0.536 | $5.83 \times 10^{-12}$ | -2.09 | 1.58 | 0.183 | $3.94 \times 10^{-14}$ | 0.933 | 1.145 | 0.037 | 0.148 | 0.060 |
| 5.5 | 0.0 | A | -2.35 | -0.668 | 0.148 | 1.96 | $4.82 \times 10^{-14}$ | -1.57 | 1.10 | 0.198 | $4.24 \times 10^{-14}$ | 0.889 | 1.076 | 0.034 | 0.110 | 0.043 |
| 5.5 | 1.0 | A | -2.12 | -0.670 | 0.0686 | 1.35 | $3.65 \times 10^{-13}$ | -1.57 | 1.25 | 0.197 | $4.00 \times 10^{-14}$ | 0.848 | 1.078 | 0.034 | 0.115 | 0.043 |
| 5.5 | 2.0 | A | -1.94 | -0.853 | 0.0786 | 0.921 | $2.57 \times 10^{-13}$ | -1.55 | 1.33 | 0.195 | $4.05 \times 10^{-14}$ | 0.804 | 1.095 | 0.032 | 0.118 | 0.044 |
| 5.5 | 3.0 | A | -1.61 | -0.722 | 0.0418 | 0.720 | $7.58 \times 10^{-13}$ | -1.59 | 2.12 | 0.193 | $3.20 \times 10^{-14}$ | 0.768 | 1.118 | 0.033 | 0.128 | 0.049 |
| 4.0 | 0.0 | B | -2.62 | -0.0144 | 0.0187 | 5.74 | $6.46 \times 10^{-12}$ | -2.01 | 0.894 | 0.198 | $4.95 \times 10^{-14}$ | ... | ... | 0.011 | 0.042 | ... |
| 4.0 | 1.0 | B | -2.52 | -0.0541 | 0.0366 | 6.65 | $1.08 \times 10^{-12}$ | -2.11 | 1.58 | 0.197 | $3.69 \times 10^{-14}$ | ... | ... | 0.011 | 0.043 | ... |
| 4.0 | 2.0 | B | -2.36 | -0.0957 | 0.0305 | 6.44 | $1.62 \times 10^{-12}$ | -2.05 | 1.19 | 0.197 | $4.37 \times 10^{-14}$ | ... | ... | 0.011 | 0.042 | ... |
| 4.0 | 3.0 | B | -2.09 | -0.193 | 0.0199 | 4.60 | $4.21 \times 10^{-12}$ | -2.10 | 1.64 | 0.198 | $3.63 \times 10^{-14}$ | ... | ... | 0.011 | 0.044 | ... |
| 4.0 | 4.0 | B | -1.96 | -0.813 | 0.0693 | 3.48 | $2.95 \times 10^{-13}$ | -2.11 | 2.10 | 0.198 | $3.13 \times 10^{-14}$ | ... | ... | 0.017 | 0.056 | ... |
| 5.5 | 0.0 | B | -2.80 | 0.0356 | 0.0203 | 3.43 | $2.74 \times 10^{-12}$ | -1.09 | -0.370 | 0.218 | $1.17 \times 10^{-13}$ | ... | ... | 0.017 | 0.092 | ... |
| 5.5 | 1.0 | B | -2.67 | 0.0129 | 0.0134 | 3.44 | $7.25 \times 10^{-12}$ | -1.14 | -0.195 | 0.216 | $1.05 \times 10^{-13}$ | ... | ... | 0.017 | 0.088 | ... |
| 5.5 | 2.0 | B | -2.45 | -0.00132 | 0.0275 | 5.14 | $8.79 \times 10^{-13}$ | -1.08 | -0.336 | 0.216 | $1.17 \times 10^{-13}$ | ... | ... | 0.017 | 0.085 | ... |
| 5.5 | 3.0 | B | -1.90 | -0.0517 | 0.0120 | 7.28 | $2.86 \times 10^{-12}$ | -1.13 | -0.109 | 0.211 | $1.04 \times 10^{-13}$ | ... | ... | 0.017 | 0.082 | ... |

[a]See equations (4) and (5). In all cases, we take $a_{c,s} = 0.1\mu$m.

[b]$R_V = A(V)/E_{B-V}$, ratio of visual extinction to reddening

[c]C abundance in double log-normal very small grain population (see equations 2 and 3)

[d]Total grain volumes in the carbonaceous and silicate populations, normalized to their abundance/depletion-limited values ($2.07 \times 10^{-27}$ and $2.98 \times 10^{-27}\,\mathrm{cm^3\,H^{-1}}$, respectively)

[e]$\chi^2_1 = \sum_i (\ln A_{\rm obs} - \ln A_{\rm mod})^2/\sigma_i^2$, for 100 points equally spaced in $\ln\lambda$

[f]$\chi^2_2 = \sum_i (\ln A_{\rm obs} - \ln A_{\rm mod})^2$

[g]$\chi^2 = \chi^2_1 + 0.4(\tilde{V}_g - 1)^{1.5} + 0.4(\tilde{V}_s - 1)^{1.5}$

Table 2. Grain Size Distribution Parameter Values for HD 210121[a]

| $10^5 b_C$[b] | $\alpha_g$ | $\beta_g$ | $a_{t,g}$ ($\mu$m) | $a_{c,g}$ ($\mu$m) | $C_g$ | $\alpha_s$ | $\beta_s$ | $a_{t,s}$ ($\mu$m) | $C_s$ | $\tilde{V}_g$[c] | $\tilde{V}_s$[c] | $\chi_1^2$[d] | $\chi_2^2$[e] | $\chi^2$[f] |
|---|---|---|---|---|---|---|---|---|---|---|---|---|---|---|
| 0.0 | -2.22 | -0.0960 | 0.00544 | 0.651 | $1.71 \times 10^{-10}$ | -1.96 | -5.23 | 0.0999 | $2.32 \times 10^{-12}$ | 0.752 | 1.407 | 0.071 | 0.080 | 0.175 |
| 1.0 | -2.18 | -0.0818 | 0.00551 | 0.614 | $1.28 \times 10^{-10}$ | -1.98 | -5.25 | 0.105 | $1.99 \times 10^{-12}$ | 0.745 | 1.415 | 0.070 | 0.078 | 0.177 |
| 2.0 | -2.04 | -0.137 | 0.00731 | 0.566 | $5.37 \times 10^{-11}$ | -1.96 | -6.05 | 0.110 | $1.97 \times 10^{-12}$ | 0.736 | 1.423 | 0.069 | 0.077 | 0.179 |
| 3.0 | -1.87 | -0.190 | 0.00911 | 0.492 | $2.40 \times 10^{-11}$ | -1.94 | -6.99 | 0.112 | $2.09 \times 10^{-12}$ | 0.726 | 1.428 | 0.072 | 0.082 | 0.184 |
| 4.0 | -1.69 | -0.264 | 0.0126 | 0.449 | $8.60 \times 10^{-12}$ | -1.90 | -9.22 | 0.119 | $2.26 \times 10^{-12}$ | 0.715 | 1.442 | 0.077 | 0.088 | 0.194 |

[a]See equations (4) and (5). In all cases, we take $a_{c,s} = 0.1\mu$m.

[b]C abundance in double log-normal very small grain population (see equations 2 and 3)

[c]Total grain volumes in the carbonaceous and silicate populations, normalized to their abundance/depletion-limited values ($2.07 \times 10^{-27}$ and $2.98 \times 10^{-27}$ cm$^3$ H$^{-1}$, respectively)

[d]$\chi_1^2 = \sum_i (\ln A_{obs} - \ln A_{mod})^2/\sigma_i^2$, for 100 points equally spaced in $\lambda^{-1}$

[e]$\chi_2^2 = \sum_i (\ln A_{obs} - \ln A_{mod})^2$

[f]$\chi^2 = \chi_1^2 + 0.4(\tilde{V}_g - 1)^{1.5} + 0.4(\tilde{V}_s - 1)^{1.5}$

Table 3. Size Distribution Parameter Values for the Magellanic Clouds[a]

| Environment | $10^5 b_{\rm C}$[b] | $\alpha_{\rm g}$ | $\beta_{\rm g}$ | $a_{\rm t,g}$ ($\mu$m) | $a_{\rm c,g}$ ($\mu$m) | $C_{\rm g}$ | $\alpha_{\rm s}$ | $\beta_{\rm s}$ | $a_{\rm t,s}$ ($\mu$m) | $C_{\rm s}$ | $\tilde{V}_{\rm g}$[d] | $\tilde{V}_{\rm s}$[d] | $\chi^2_1$[e] | $\chi^2_2$[f] | $\chi^2$[g] |
|---|---|---|---|---|---|---|---|---|---|---|---|---|---|---|---|
| LMC avg | 0.0 | -2.91 | 0.895 | 0.578 | 1.21 | $7.12 \times 10^{-17}$ | -2.45 | 0.125 | 0.191 | $1.84 \times 10^{-14}$ | 0.401 | 0.675 | 0.025 | 0.069 | 0.025 |
| LMC avg | 1.0 | -2.99 | 2.46 | 0.0980 | 0.641 | $3.51 \times 10^{-15}$ | -2.49 | 0.345 | 0.184 | $1.78 \times 10^{-14}$ | 0.330 | 0.687 | 0.018 | 0.033 | 0.018 |
| LMC avg | 2.0 | 4.43 | 0.0 | 0.00322 | 0.285 | $9.57 \times 10^{-24}$ | -2.70 | 2.18 | 0.198 | $7.29 \times 10^{-15}$ | 0.279 | 0.758 | 0.016 | 0.019 | 0.016 |
| LMC 2 | 0.0 | -2.94 | 5.22 | 0.373 | 0.349 | $9.92 \times 10^{-17}$ | -2.34 | -0.243 | 0.184 | $3.18 \times 10^{-14}$ | 0.263 | 0.753 | 0.025 | 0.043 | 0.025 |
| LMC 2 | 0.5 | -2.82 | 9.01 | 0.392 | 0.269 | $6.20 \times 10^{-17}$ | -2.36 | -0.113 | 0.182 | $3.03 \times 10^{-14}$ | 0.252 | 0.765 | 0.022 | 0.037 | 0.022 |
| LMC 2 | 1.0 | 4.16 | 0.0 | 0.342 | 0.0493 | $3.05 \times 10^{-15}$ | -2.44 | 0.254 | 0.188 | $2.24 \times 10^{-14}$ | 0.206 | 0.820 | 0.012 | 0.014 | 0.012 |
| SMC bar | 0.0 | -2.79 | 1.12 | 0.0190 | 0.522 | $8.36 \times 10^{-14}$ | -2.26 | -3.46 | 0.216 | $3.16 \times 10^{-14}$ | 0.254 | 1.308 | 0.017 | 0.019 | 0.027 |

[a]See equations (4) and (5). In all cases, we take $a_{\rm c,s} = 0.1\mu$m.

[b]C abundance in double log-normal very small grain population (see equations 2 and 3)

[d]Total grain volumes in the carbonaceous and silicate populations, normalized to their abundance/depletion-limited values (1.29, 1.86, 0.518, and 0.745 $\times 10^{-27}\,{\rm cm^3\,H^{-1}}$ for carbonaceous in LMC, silicate in LMC, carbonaceous in SMC, and silicate in SMC, respectively)

[e]$\chi^2_1 = \sum_i (\ln A_{\rm obs} - \ln A_{\rm mod})^2/\sigma_i^2$, for 100 points equally spaced in $\lambda^{-1}$.

[f]$\chi^2_2 = \sum_i (\ln A_{\rm obs} - \ln A_{\rm mod})^2$

[g]$\chi^2 = \chi^2_1 + 0.4(\tilde{V}_{\rm g} - 1)^{1.5} + 0.4(\tilde{V}_{\rm s} - 1)^{1.5}$